expression vectors coding myc-His tagged MPF (Fig. 1C, lane 2) and the full length of mesothelin variant 1 (Fig. 1C, lane 3). A smaller band on lane 3 compared to the myc-His tagged MPF on lane 2 were detected by both anti-MPF Abs. MPF and mesothelin are produced together as a precursor form. Following cleavage by a protease furin, MPF is released as an N-terminal 31-kDa fragment from mesothelin [15]. The smaller band on the lane 3 seems to be the 31-kDa mature form of MPF without myc-His Tag. A sandwich ELISA for MPF was constructed using the anti-MPF antibodies 20–10 and 41–28. The standard curve using purified recombinant MPF was shown in Fig. 2A. Correlated with Fig. 1C, the MPF sandwich ELISA detected the antigen in the culture supernatant of the 293T transfectant expressing the full length of mesothelin variant 1 (Fig. 2C, MPF/MSLN-293T), as well as MPF-transfected cells (Fig. 2C, MPF-293T) but not the soluble mesothelin secreted in the culture supernatant of the MSLN-transfectants (Fig. 2C, MSLN-293T).

The monoclonal anti-MSLN antibody, clone 11–25, were generated by immunizing mice with recombinant MSLN (amino acids 297–580 of mesothelin variant 1). The specificity of 11–25 to MSLN was tested using a lung cancer cell line, NCI-H226, which has been clarified to express mesothelin [14]. 11–25 detected not only the antigen on the cell surface of NCI-H226 by flowcytometory (Fig. 1E, upper left panel), but also identified soluble antigen in the culture supernatant of NCI-H226 by immunoprecipitation (Fig. 1F, lane 11–25). Another anti-MSLN Ab, clone MN, which the Pastan's laboratory has previously developed, was used, in combination with 11–25, to establish a sandwich ELISA for MSLN [14]. The standard curve using recombinant MSLN was shown in Fig. 2B. The MSLN sandwich ELISA recognized the soluble antigen in the culture supernatant of NCI-H226 (Fig. 2C, H226) as well as the 293T transfectant expressing the full length of mesothelin variant1 (Fig. 2C, MPF/MSLN-293T). On the other hands, this MSLN ELISA did not detect recombinant MPF in the culture supernatant of the MPF-transfectants (Fig. 2C, MPF-293T).

3.2. MPF and MSLN in blood samples

We measured serum MPF and MSLN levels in all subjects. Serum MPF levels differed among the five groups (Fig. 3A and Table 1), with mean serum MPF values were higher for MPM patients (68.7 ± 101.1 ng/ml [mean ± standard deviation]) than for patients with lung cancer (16.6 ± 15.3 ng/ml), individuals with other cancers (15.1 ± 9.7 ng/ml), healthy asbestos-exposed subjects (9.7 ± 5.3 ng/ml) and healthy adults (9.0 ± 2.9 ng/ml). The difference in median values between MPM and every control group was statistically significant (Mann–Whitney's U test; $p < 0.001$). Mean serum MSLN levels in MPM, patients with lung cancer, individuals with other cancers, healthy asbestos-exposed subjects, or healthy adults were 130.0 ± 112.9 ng/ml, 83.4 ± 50.4 ng/ml, 74.4 ± 45.3 ng/ml, 59.5 ± 25.6 ng/ml and 61.4 ± 21.4 ng/ml, respectively (Fig. 3B and Table 1). The median serum MSLN level of MPM was significantly higher than in the control groups (Mann–Whitney's U test; MPM *vs.* lung cancer: $p = 0.028$, MPM *vs.* other cancers: $p = 0.005$, MPM *vs.* asbestos-exposed subjects: $p = 0.010$, MPM *vs.* healthy adults: $p < 0.001$). There was no significant difference in MPF or MSLN levels among MPM patients with different histologies (Table 1).

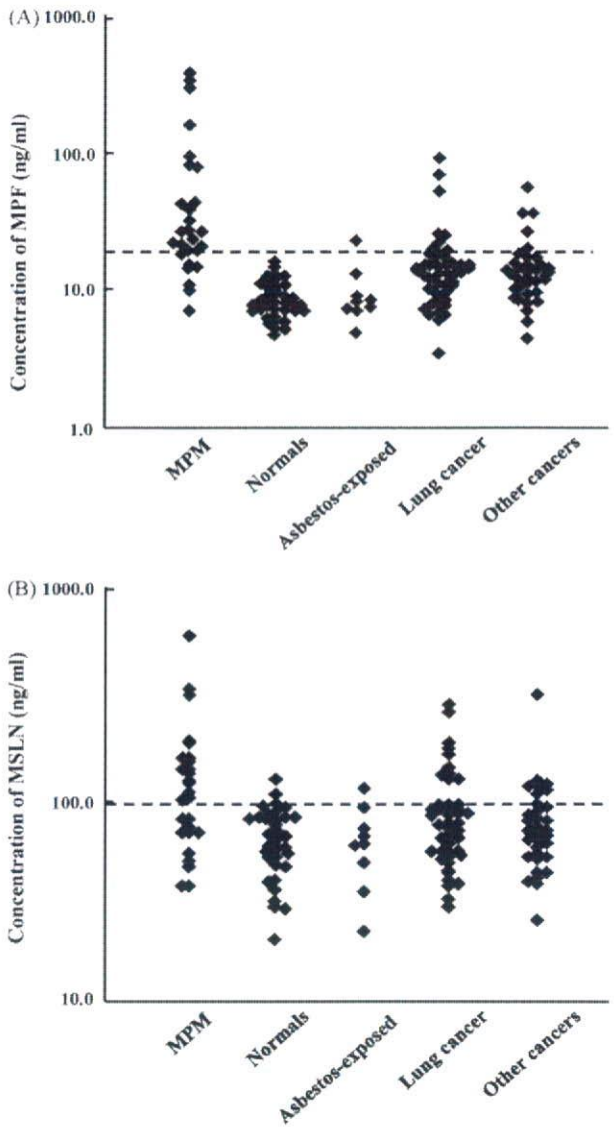

Fig. 3 Megakaryocyte potentiating factor (MPF) (A) and mesothelin variants (MSLN) (B) levels in the sera of malignant pleural mesothelioma (MPM) patients and control groups. Each dot represents one patient. The horizontal broken lines represent cut-off values: 19.1 ng/ml for MPF and 93.5 ng/ml for MSLN. MPM, malignant pleural mesothelioma; Normals, healthy volunteers; Asbestos-exposed, asbestos-exposed asymptomatic individuals; other cancers, ovarian, stomach and colon cancer patients.

3.3. Cut-off value, sensitivities and specificities calculation of MPF and MSLN

To assess the clinical potential of MPF, we compared sensitivities and specificities of MPF with those of MSLN. The operating characteristics for the two tumor markers with their cut-off points for achieving the best individual accuracy are shown in Fig. 4A. The area under the receiver operating characteristic (ROC) curve (AUC) for serum MPF

Table 1 Serum concentrations of megakaryocyte potentiating factor (MPF) and mesothelin variants (MSLN) in mesothelioma patients and controls

Diagnosis	Number of study participants	MPF (ng/ml)			MSLN (ng/ml)		
		Mean (S.D.)	Median	Range	Mean (S.D.)	Median	Range
MPM	27	68.7 (101.1)	26.3	6.9–370.1	130.0 (112.9)	101.5	35.9–576.1
Epithelial type	13	87.4 (112.6)	38.1	14.2–370.1	132.2 (67.7)	129.3	64.8–317.8
Sarcomatoid type	3	16.5 (5.8)	19.1	9.8–20.4	67.9 (38.6)	57.3	44.5–112.4
Mixed type	5	77.7 (143.7)	14.8	6.9–334.6	158.8 (233.6)	65.2	35.9–576.1
Unclassified type	6	47.0 (54.3)	24.7	15.3–156.3	132.3 (88.9)	109.7	35.9–296.6
Malignant condition							
Lung cancer	47	16.6 (15.3)	13.3*	3.4–89.4	83.4 (50.4)	70.7†	28.6–267.8
Other cancers	35	15.1 (9.7)	13.0*	4.4–54.5	74.4 (45.3)	66.4‡	24.6–298.2
Ovarian cancer	18	18.0 (12.5)	13.7	4.4–54.5	83.2 (56.9)	67.8	41.7–298.2
Stomach cancer	8	14.3 (3.7)	14.1	9.6–19.7	73.9 (29.0)	69.9	36.9–113.8
Colon cancer	9	9.7 (2.9)	8.7	5.8–14.0	57.0 (24.5)	51.6	24.6–106.6
Asbestos-exposed individuals	9	9.7 (5.3)	8.2*	4.9–22.7	59.5 (25.6)	56.7§	21.6–106.0
Healthy volunteers	38	9.0 (2.9)	8.0*	4.8–16.6	61.4 (21.4)	62.0*	19.6–117.4

* Significance of median values for the specified control groups compared with MPM. Mann–Whitney's *U* test; $p < 0.001$.
† Significance of median values for the specified control groups compared with MPM. Mann–Whitney's *U* test; $p = 0.028$.
‡ Significance of median values for the specified control groups compared with MPM. Mann–Whitney's *U* test; $p = 0.005$.
§ Significance of median values for the specified control groups compared with MPM. Mann–Whitney's *U* test; $p = 0.01$.

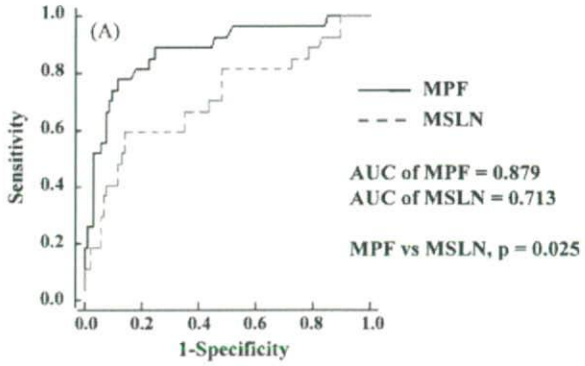

Marker	Cut-off (ng/ml) (n=94)	Sensitivity (%)	Specificity (%)
MPF	19.1	74.1	90.4
MSLN	93.5	59.3	86.2

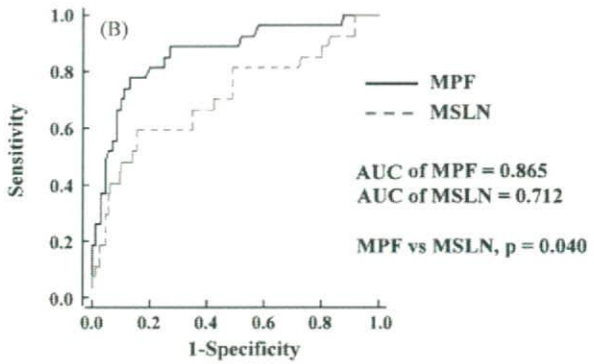

Marker	Cut-off (ng/ml) (n=129)	Sensitivity (%)	Specificity (%)
MPF	19.1	74.1	89.1
MSLN	123.7	40.7	93.8

Fig. 4 Receiver operating characteristic (ROC) curves for megakaryocyte potentiating factor (MPF) and mesothelin variants (MSLN) for differentiation between malignant pleural mesothelioma ($n = 27$) and controls. Controls comprise lung cancer patients ($n = 47$), asbestos-exposed asymptomatic individuals ($n = 9$) and healthy volunteers ($n = 38$) for (A). For the analysis shown in (B), control groups include other cancers ($n = 35$) in addition to those specified in (A). The tables show the best statistical cut-off values for MPF and MSLN with pairs of sensitivity and specificity.

was 0.879 for differentiating MPM patients from controls comprising lung cancer patients, asbestos-exposed individuals and healthy adults, with a cut-off value of 19.1 ng/ml (sensitivity = 74.1%, specificity = 90.4%), whereas the AUC for serum MSLN was 0.713 with a cut-off value of 93.5 ng/ml (sensitivity = 59.3%, specificity = 86.2%) (Fig. 4A). Serum MPF levels were elevated in 20 (74.1%) MPM patients, eight (17.0%) lung cancer patients and five (14.3%) individuals with other cancers (Fig. 3A). Corresponding serum MSLN levels were elevated in 59.3%, 21.3% and 20.0% of the patients (Fig. 3B). Both MPF and MSLN showed elevated levels in

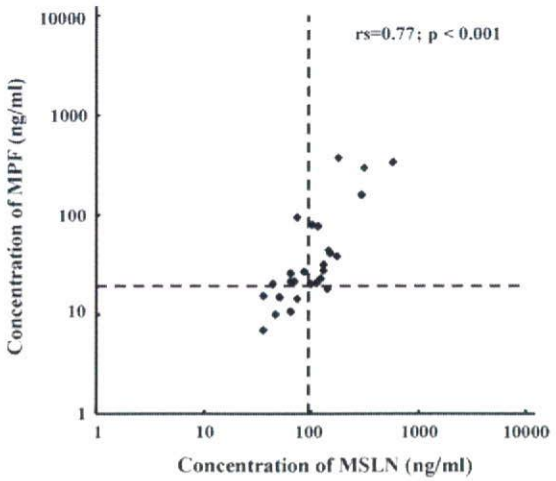

Fig. 5 Inter-marker correlation between megakaryocyte potentiating factor (MPF) and mesothelin variants (MSLN) for malignant pleural mesothelioma (MPM). Each dot indicates MPF and MSLN values for the same MPM patient ($n = 27$). r_s, Pearson's correlation coefficient. The horizontal dotted line represents the cut-off value for MPM (19.1 ng/ml) and the vertical dotted line for MSLN (93.5 ng/ml).

four (22.2%) ovarian cancer patients, while MPF values were elevated in one (11.1%) asbestos-exposed adult and none of the healthy donors, and MSLN levels were elevated in one (11.1%) asbestos-exposed adult and two (5.3%) healthy donors. Calculation of areas under the ROC curves showed a significant difference between the two markers ($p = 0.025$) (Fig. 4A). ROC curves for a comparison of MPM with all non-MPM patients and healthy adults, yielded an AUC of 0.865 for MPF and of 0.712 for MSLN (MPF *vs.* mesothelin, $p = 0.04$) (Fig. 4B). Sensitivity of MSLN decreased to 40.7% while that of MPF did not change (Fig. 4B). Comparison of the AUC values thus showed a better diagnostic performance by MPF than MSLN for discriminating MPM.

3.4. Inter-marker correlation

To examine inter-marker correlation between MPF and MSLN values for MPM, we plotted concentrations of MPF and MSLN in the same figure (Fig. 5) and found a significant correlation between MPF and MSLN values for MPM (Pearson's correlation coefficient, $r_s = 0.77$; $p < 0.001$). Concentrations for six patients were above the cut-off value for MPF (19.1 ng/ml) but below the cut-off values (93.5 ng/ml) for MSLN, whereas only one showed the opposite condition. Concentrations for 14 patients were above the cut-off values for both markers and for six patients they were below these values (Fig. 5).

4. Discussion

Recent studies identified increased levels of MSLN in the blood of MPM [11,16–18] and other histological cancer patients [9,10]. They suggested MSLN was useful for diagnosis of MPM and for monitoring disease progression. Recently, MPM patients were found to have raised serum concentrations of MPF [13,19], indicating that MPF can also be a candidate diagnostic marker for MPM. To determine which molecule, MPF or MSLN, is more sensitive for screening of MPM, we developed two novel sets of ELISA system. The one for MSLN recognizes mesothelin variants 1 and 3. In our study, higher MPF levels were found in 74.1% of MPM patients and elevated MSLN levels in 59.3%. Scherpereel et al. demonstrated that MPM epithelioid type had significant elevated values for MSLN than mixed type or sarcomatoid type [17]. Nevertheless, we and Creaney et al. did not find significant difference in levels of either MSLN or MPF in MPM patients with different histologies (Table 1) [20]. The sensitivity of 59.3% of MSLN established in our study was comparable to the sensitivity of 52% in Creaney' s study of 117 MPM patients [20] or 68% of Cristaudo' s study [21]. Regarding sensitivity of MPF to patients with MPM, we do not know any other reports.

When two or more tests are available for diagnostic purposes, comparison of the respective AUCs will often show which test is the most effective. ROC curves of MPF yielded an AUC of 0.879, and those of MSLN an AUC of 0.713 (MPF *vs.* MSLN, $p = 0.025$) (Fig. 4A). There was a significant correlation between MPF an MSLN values for MPM (Pearson's correlation coefficient (r_s) = 0.77). This indicates that MPF is probably more sensitive than MSLN for diagnosis of MPM. Though osteopontin and CA125 are also indicated as potential markers in the diagnosis of MPM, neither showed better sensitivity for MPM in comparison with MSLN [20,22].

Physiological cleavage from the mesothelin precursor protein at the furin cleavage site may be responsible for extracellular secretion of MPF [13]. Mesothelin and its variants, attached to cell membranes by GPI-anchors, are also readily released *in vivo*, but the mechanism of mesothelin release has not yet been identified. We transfected the full length of mesothelin variant 1 cDNA into 293 cells and part of mesothelin variant 1 is released from the cell surface and can be measured with the ELISA system (Fig. 2 C, MPF/MSLN-293T). A relevant example is carcinoembryonic antigen (CEA), a tumor-associated GPI-anchored glycoprotein that is commonly shed from the cell surface [23]. The as yet unknown process that mediates a release of the membrane-bound mesothelin variant 1 may be associated with the lower sensitivity of MSLN in comparison with that of MPF. However, additional studies are needed to identify and characterize the process of mesothelin secretion.

Just as MPF and mesothelin originate from the same mesothelin precursor, so adrenomedullin (ADM) and proadrenomedulin (PAMP) are potent vasodilatory peptides derived from a common precursor peptide. However, their short half-life and the presence of a binding protein have been obstacles for an accurate quantification. The ADM precursor is produced in quantities stoichiometric to ADM and PAMP, but is non-functional and stable, while the quantities of the ADM precursor thus produced directly reflect those of ADM and PAMP [24]. One of the reasons for the lower sensitivity of the mesothelin assay could be a lower stability of the protein, but the stability of both proteins needs to be examined and compared.

Pastan's group showed that most ovarian cancer cells express 40-kDa protein mesothelin at the cell surface [25]. MPF was initially isolated from supernatant of pancreatic

cancer cells [26]. Scholler et al. and Hassan et al. independently demonstrated elevated levels of SMRP in 23 of 30 (76.7%) and 40 of 56 (71%) sera from patients with ovarian carcinoma by using a monoclonal antibody, OV569, that was prepared by immunizing mice with ovarian carcinoma cells [10,18]. However, Beyer et al. reported SMRP values were increased in less than 10% of 111 samples collected from ovarian cancer patients [16]. In our study, serum concentrations of both MPF and MSLN were increased in only four of 18 (22.2%) individuals with ovarian cancer. Frequent positive immunostaining for mesothelin is reportedly associated with the non-mucinous type of ovarian cancers [27,28]. Although these reports did not include a description of histological subtype classification in the various blood samples studied, the different ratios of mucinous to non-mucinous type in the samples may partly account for the differences in positivity of serum mesothelin. For MPF, ours is the first reported study of serum levels in ovarian cancer patients.

5. Conclusion

We used ELISA systems developed by us to detect significant differences in the levels of serum MPF and MSLN between MPM patients and controls including lung cancer patients, asbestos-exposed individuals, and normal volunteers. In addition, it is suggested that MPF has superior specificity for MPM compared to MSLN. We are planning a further study to determine the relationship between serum MPF and disease stage, prognosis and histological subtypes.

Conflict of interest

None.

Acknowledgements

The following medical institute and investigator was involved in the study: The First Department of Internal Medicine, Faculty of Medicine, University of Toyama (Ryuji Hayashi).

References

[1] Vogelzang NJ, Rusthoven JJ, Symanowski J, Denham C, Kaukel E, Ruffie P, et al. Phase III study of pemetrexed in combination with cisplatin versus cisplatin alone in patients with malignant pleural mesothelioma. J Clin Oncol 2003;21:2636–44.
[2] Stahel RA. Malignant pleural mesothelioma: a new standard of care. Lung Cancer 2006;54(Suppl 2):S9–14.
[3] Pelucchi C, Malvezzi M, La Vecchia C, Levi F, Decarli A, Negri E. The Mesothelioma epidemic in Western Europe: an update. Br J Cancer 2004;90:1022–4.
[4] Leithner K, Leithner A, Clar H, Weinhaeusel A, Radl R, Krippl P, et al. Mesothelioma mortality in Europe: impact of asbestos consumption and simian virus 40. Orphanet J Rare Dis 2006;1:44.
[5] Murayama T, Takahashi K, Natori Y, Kurumatani N. Estimation of future mortality from pleural malignant mesothelioma in Japan based on an age-cohort model. Am J Ind Med 2006;49:1–7.
[6] Leigh J, Driscoll T. Malignant mesothelioma in Australia, 1945–2002. Int J Occup Environ Health 2003;9:206–17.
[7] Chang K, Pastan I. Molecular cloning of mesothelin, a differentiation antigen present on mesothelium, mesotheliomas, and ovarian cancers. Proc Natl Acad Sci USA 1996;93:136–40.
[8] Muminova ZE, Strong TV, Shaw DR. Characterization of human mesothelin transcripts in ovarian and pancreatic cancer. BMC Cancer 2004;4:19.
[9] Hellstrom I, Raycraft J, Kanan S, Sardesai NY, Verch T, Yang Y, et al. Mesothelin variant 1 is released from tumor cells as a diagnostic marker. Cancer Epidemiol Biomarkers Prev 2006;15:1014–20.
[10] Scholler N, Fu N, Yang Y, Ye Z, Goodman GE, Hellstrom KE, et al. Soluble member(s) of the mesothelin/megakaryocyte potentiating factor family are detectable in sera from patients with ovarian carcinoma. Proc Natl Acad Sci USA 1999;96:11531–6.
[11] Robinson BW, Creaney J, Lake R, Nowak A, Musk AW, de Klerk N, et al. Mesothelin-family proteins and diagnosis of mesothelioma. Lancet 2003;362:1612–6.
[12] Shiomi K, Miyamoto H, Segawa T, Hagiwara Y, Ota A, Maeda M, et al. Novel ELISA system for detection of N-ERC/mesothelin in the sera of mesothelioma patients. Cancer Sci 2006;97:928–32.
[13] Onda M, Nagata S, Ho M, Bera TK, Hassan R, Alexander RH, et al. Megakaryocyte potentiation factor cleaved from mesothelin precursor is a useful tumor marker in the serum of patients with mesothelioma. Clin Cancer Res 2006;12:4225–31.
[14] Onda M, Willingham M, Nagata S, Bera TK, Beers R, Ho M, et al. New monoclonal antibodies to mesothelin useful for immunohistochemistry, fluorescence-activated cell sorting, Western blotting, and ELISA. Clin Cancer Res 2005;11:5840–6.
[15] Hassan R, Bera T, Pastan I. Mesothelin: a new target for immunotherapy. Clin Cancer Res 2004;10:3937–42.
[16] Beyer HL, Geschwindt RD, Glover CL, Tran L, Hellstrom I, Hellstrom KE, et al. MESOMARK: a potential test for malignant pleural mesothelioma. Clin Chem 2007;53:666–72.
[17] Scherpereel A, Grigoriu B, Conti M, Gey T, Gregoire M, Copin MC, et al. Soluble mesothelin-related peptides in the diagnosis of malignant pleural mesothelioma. Am J Respir Crit Care Med 2006;173:1155–60.
[18] Hassan R, Remaley AT, Sampson ML, Zhang J, Cox DD, Pingpank J, et al. Detection and quantitation of serum mesothelin, a tumor marker for patients with mesothelioma and ovarian cancer. Clin Cancer Res 2006;12:447–53.
[19] Maeda M, Hino O. Molecular tumor markers for asbestos-related mesothelioma: serum diagnostic markers. Pathol Int 2006;56:649–54.
[20] Creaney J, van Bruggen I, Hof M, Segal A, Musk AW, de Klerk N, et al. Combined CA125 and mesothelin levels for the diagnosis of malignant mesothelioma. Chest 2007;132:1239–46.
[21] Cristaudo A, Foddis R, Vivaldi A, Guglielmi G, Dipalma N, Filiberti R, et al. Clinical significance of serum mesothelin in patients with mesothelioma and lung cancer. Clin Cancer Res 2007:5076–81.
[22] Grigoriu BD, Scherpereel A, Devos P, Chahine B, Letourneux M, Lebailly P, et al. Utility of osteopontin and serum mesothelin in malignant pleural mesothelioma diagnosis and prognosis assessment. Clin Cancer Res 2007;13:2928–35.
[23] Khan WN, Hammarstrom S. Biosynthesis of carcinoembryonic antigen (CEA) gene family members expressed in human tumor cell lines: evidence for cleavage of the glycosyl phosphatidyl inositol (GPI) anchor by GPI-PLC and GPI-PLD. Biochem Int 1991;25:723–31.
[24] Ernst A, Hellmich S, Bergmann A. Proneurotensin 1–117, a stable neurotensin precursor fragment identified in human circulation. Peptides 2006;27:1787–93.
[25] Chang K, Pai LH, Batra JK, Pastan I, Willingham MC. Characterization of the antigen (CAK1) recognized by monoclonal

antibody K1 present on ovarian cancers and normal mesothelium. Cancer Res 1992;52:181–6.
[26] Yamaguchi N, Hattori K, Oh-eda M, Kojima T, Imai N, Ochi N. A novel cytokine exhibiting megakaryocyte potentiating activity from a human pancreatic tumor cell line HPC-Y5. J Biol Chem 1994;269:805–8.
[27] Chang K, Pastan I, Willingham MC. Isolation and characterization of a monoclonal antibody, K1, reactive with ovarian cancers and normal mesothelium. Int J Cancer 1992;50: 373–81.
[28] Ordonez NG. Application of mesothelin immunostaining in tumor diagnosis. Am J Surg Pathol 2003;27:1418–28.

DOI 10.1002/prca.200700119 *Proteomics Clin. Appl.* 2008, *2*, 1246–1254

RESEARCH ARTICLE

Aberrant expression of glycosylation in juvenile gastrointestinal stromal tumors

Tsuyoshi Takahashi[1], Tetsuji Naka[2], Minoru Fujimoto[2], Satoshi Serada[2], Jirou Horino[3], Fumitaka Terabe[3], Seiichi Hirota[4], Eiji Miyoshi[5], Toshihiro Hirai[6], Kiyokazu Nakajima[1], Akiko Nishitani[7], Yoshihito Souma[1], Yoshiki Sawa[1] and Toshirou Nishida[1]

[1] Department of Surgery, Osaka University Graduate School of Medicine, Suita, Japan
[2] Laboratory for Immune Signal, National Institute of Biomedical Innovation, Ibaraki, Japan
[3] Department of Gastroenterology and Hepatology, Osaka University Graduate School of Medicine, Suita, Japan
[4] Department of Surgical Pathology, Hyogo College of Medicine, Nishinomiya, Japan
[5] Department of Molecular Biochemistry and Clinical Investigation, Osaka University Graduate School of Medicine, Suita, Japan
[6] Department of Surgery, Division of Gastroenterology, Kawasaki Medical School, Kurashiki, Japan
[7] Department of Surgery, National Hospital Organization Kure Medical Center, Kure, Japan

Most adult gastrointestinal stromal tumors (GIST) are thought to be caused by activating mutations in the *KIT* or *PDGFRA* gene. However, many juvenile GIST lack either mutation and are considered to develop with a different pathogenesis. To investigate the molecular characteristics of juvenile GIST, we analyzed the proteome difference in phosphorylated protein between adult and juvenile GIST. Eleven GIST samples (seven adult cases and four juvenile cases lacking either mutation) were analyzed by using immunostaining and LC-MS/MS. Comparative analysis of tyrosine-phosphorylated protein levels showed that juvenile GIST possessed phosphorylated KIT in spite of lacking mutation in the *KIT* gene. Moreover, downstream signals of KIT were also activated as in adult GIST. Although, SDS-PAGE gels showed that there was a difference of each KIT bands between adult and juvenile GIST, they became the same after removal of N-glycans or sialic acids. Moreover, one of the most typical enzymes, ST6Gal1, which transfers Neu5Ac residues in α2-6 linkage to Gal β1-4GlcNAc units on N-glycans, is significantly less expressed in juvenile GIST. This suggests that the difference in KIT is generated by post-translational modification and may play a role in the progression of juvenile GIST.

Received: November 15, 2007
Revised: March 3, 2008
Accepted: March 24, 2008

Keywords:
Glycosylation / Juvenile GIST / KIT / Mass spectrometer / ST6Gal1

Correspondence: Dr. Toshirou Nishida, Department of Surgery, Osaka University Graduate School of Medicine, Suita, Japan
E-mail: toshin@surg1.med.osaka-u.ac.jp
Fax: +81-6-6879-3163

Abbreviations: **GIST**, gastrointestinal stromal tumor(s); **RTK**, receptor tyrosine kinase

1 Introduction

Gastrointestinal stromal tumors (GIST) are the most common mesenchymal neoplasms of the gastrointestinal tract in adults [1, 2]. They are thought to originate from interstitial cells of Cajal (ICC) or an ICC precursor, since both have

similar ultrastructural features and express the KIT receptor tyrosine kinase (RTK) [1, 3]. In over 80% of all cases, GIST feature activating mutations in *KIT*, which encode class III RTK [1, 4, 5]. These mutations can result in ligand-independent kinase activity and auto-phosphorylation of KIT. We previously reported that germ-line gain-of-function mutations at exon 11, 13, or 17 of the c-kit gene caused familial and multiple GIST [6–8], so that these gain-of-function mutations are considered a cause of GIST. Recently, the presence of activating mutations in *PDGFRA* has been reported in a subset of GIST lacking *KIT* mutations, and these mutations appear to contribute to the development of GIST through a similar pathway [9, 10]. KIT and PDGFRA belong to the same subfamily of type III RTK. Thus, activating mutations in these two genes can be regarded as alternative oncogenic mechanisms for GIST. Although most GIST have mutually exclusive activating mutations in either of these two genes, a very small number of GIST subsets have no mutations in either of these two genes (about 5%). These subsets includes neurofibromatosis type1 [11], Carney's triad [12, 13], and juvenile type [14–17]. Findings of studies into the pathogenesis of neurofibromatosis type1 and Carney's triad have been reported recently, but no reports have been published on the pathogenesis of juvenile GIST.

GIST typically occur in adults over the age of 40, with a peak incidence between 60 and 70 years of age [18]. Although the clinicopathologic and molecular characteristics of GIST in adults have been well characterized, few data on juvenile GIST are available. Some investigators have reported that they differ from older adult cases in clinical and pathologic findings [15–17], while anecdotal reports of sporadic juvenile GIST suggest that an epithelioid morphology and wild-type *KIT* and *PDGFRA* in genotype are common findings [14, 19]. Most adult GIST, however, feature spindle morphology and *KIT*-mutations, usually involving the juxtamembrane domain (exon 11). Juvenile GIST are therefore thought to have a different pathogenesis from that of adult GIST.

In this study, we performed a proteomic expression analysis of juvenile GIST to explore alternative RTK oncoproteins of juvenile GIST that may participate in their pathogenesis.

2 Materials and methods

2.1 Patients

This study was performed in accordance with the authors' institutional guidelines and was approved by the institutional review board. Written informed consent was obtained in the case of living patients. Seven patients with GIST, who were less than 30-years-old at diagnosis and were treated at Osaka University Hospital between 1998 and 2006, were enrolled in this study. In addition to pediatric GIST patients defined as younger than 18 years of age, we included young adult patients (older than 18 but less than 30) in this study, because this group is reportedly more similar to the pediatric than the adult subset [14]. Seven adult GIST patients were enrolled in this study as a control group. All samples were fixed in formalin, and paraffin sections (3-μm thick) were cut from the formalin-fixed tissue and used for H &E staining and immunohistochemistry. Mesenchymal tumors, which had a consistent morphology with GIST in the H&E staining and were positive for KIT and/or CD34 by immunohistochemistry, were diagnosed to be GIST.

2.2 Immunohistochemistry

Immunohistochemistry was performed as described previously [20]. Rabbit polyclonal antibody against human KIT (A4502, DAKO Cytomation, Kyoto, Japan), mouse mAb against human CD34 (NCL-END, Novocastra Laboratories, Newcastle-upon-Tyne, UK), rabbit polyclonal antibody against bovine S-100 protein and mouse mAb against human desmin (both from DAKO Cytomation) were used as the primary antibodies. Detection was performed with the Envision (+) kit HRP (DAB) System.

2.3 Mutation analysis of *KIT* and *PDGFRA* genes

Analysis of *KIT* and *PDGFRA* gene mutation was performed with PCR products of complementary DNA (cDNA) in ten cases and genomic DNA in two cases as described previously [1]. The cDNA was synthesized from fresh samples and the genomic DNA was extracted from paraffin sections (10-μm thick).

2.4 Protein extraction and preparation

GIST samples were homogenized in a sample buffer (10 mM Tris-HCl pH 7.5, 150 mM NaCl, 1 × antiprotease mixture Complete (Nacalai Tesque, Kyoto, Japan), 1% NP-40, 0.1% SDS, 0.1% sodium deoxycholate, 2% tritonX-100, 1 μM sodium orthovanadate), and stored at -80°C until use. The RC-DC Protein Assay Kit (Bio-Rad Laboratories, Hercules, CA) was used to establish a final protein concentration of 5.0 mg/mL.

For immunoprecipitation, we mixed 0.5 mg of each sample with 0.5 μg mouse anti-phosphotyrosine antibody, clone 4G10 (Upstate Biotechnology, Lake Placid, NY) or 0.2 μg rabbit anti-KIT antibody (Santa Cruz Biotechnology, Santa Cruz, CA) and incubated the mixture at 4°C for 6 h. Next, we added protein G-Sepharose (Amersham Bioscience, Piscataway, NJ) and incubated the mixture at 4°C for 2 h. Finally, it was washed three times in TBS, and protein was extracted by using SDS sample buffer (0.125 M Tris-HCl pH6.8, 10% 2-mercaptoethanol, 4% SDS, 10% sucrose, 0.004% Bromophenole blue). Extracted proteins were resolved using 10% Bis-Tris Criterion XT Precast gels (Bio-Rad) and 4–10% Multigel II Mini (Daiichi Pure Chemicals, Tokyo, Japan). The gels were stained with the Silver Stain MS Kit (Wako Pure Chemical Industries, Osaka, Japan) or used for protein transfer to PVDF membrane.

For lectin precipitation, we used SSA-lectin agarose (Seikagaku, Tokyo, Japan), which is originated from Japanese Elderberry and specifically recognizes α2-6 sialic acids. We incubated 2 mg of each sample with 100 μL of SSA-lectin agarose for 8 h and washed three times with TBS and binding protein was eluted by using 0.5 M Lactose (Nacalai Tesque). All steps were performed at 4°C. Extracted proteins were resolved by using 10% Bis-Tris Criterion XT Precast gels (Bio-Rad) and 4–10% Multigel II Mini (Daiichi Pure Chemicals).

2.5 Western blotting

After transfer of the proteins to PVDF membranes (Millipore, Bedford, MA), the membranes were washed and blocked with 1% BSA (Nacalai Tesque) in PBS containing 0.1% Tween 20 (PBST). The membranes were incubated with mouse anti-phosphotyrosine antibody; clone 4G10 (Upstate Biotechnology) at a 1:2000 dilution or with a rabbit polyclonal anti-KIT antibody (Dako Cytomation) at a 1:1000 dilution. Finally, the signals were visualized by means of an ECL reaction system (Perkin Elmer Life Science, Boston, MA).

2.6 Identification of protein band

After Western blotting and silver staining, the protein bands, which corresponded to specific bands on Western blotting membranes, were excised and digested with the sequencing grade trypsin (Promega, Madison, WI) according to published procedures [21]. Digested peptides were then extracted with 5% TFA in ACN (ACN/DW, 50:45, v/v), sonicated for 5 min, and concentrated by means of evaporation. Peptides were solubilized with 0.1% TFA in ACN/DW (2:98, v/v) and analyzed by LC-MS/MS. RP separations were executed with a Magic 2002 capillary HPLC (Michrom Bioresources, Auburn, CA) with a C-18 RP column (length 15 cm, id 200 μm; GL Sciences, Tokyo, Japan). The injected peptides were then eluted by using a 30-min linear gradient of 5–65% of solvent A and solvent B (solvent A: 0.1%formic acid in ACN/DW, 2:98 v/v, solvent B: 0.1% formic acid in ACN/DW, 95:5 v/v). The column was directly interfaced to an LCQ IT mass spectrometer (ThermoElectron, San Jose, CA) equipped with a nano-electrospray ion source, and data were collected in the double mode, which was configured to alternate between a single full MS scan followed by an MS/MS scan of the most intense precursor masses. MS/MS spectra were searched against a human protein Swiss-Prot database with the aid of the MASCOT search program (Matrix Science K. K., Tokyo, Japan, ver. 2.1.03). The following parameters were used for the search: enzyme: trypsin, missed cleavage: one, variable modification: oxidation of methionines, fixed modification: carbamidomethylation of cysteines and monoisotopic peptide masses.

2.7 Cutting of glycosylation and sialylation

We used Glycopeptidase F (Takara, Otsu, Japan) to cut N-Glycans. After immunoprecipitation, we mixed 1 mU Glycopeptidase F into the samples and incubated the mixture at 37°C for 12 h. After this procedure, the band of KIT was visualized by Western blotting. We also used neuraminidase (Seikagaku, Tokyo, Japan), which was produced from *Streptococcus* sp. and digested α2-3 sialic acid, α2-6 sialic acid and α2-8 sialic acid residues. After immunoprecipitation, 100 mU/mL neuraminidase was mixed into the samples and the mixture incubated at 37°C for 3 h. Finally, the band of KIT was visualized by Western blotting.

2.8 DNA array

The GeneChip array data were compared by using the Kurabo custom analysis services by Kurabo Industries (Osaka, Japan), which is the service provider authorized by Affymetrix Japan K.K.(Tokyo, Japan).

Briefly, total RNA was reverse transcripted to c DNA with the T7 oligo d(T) primer (Affymetrix, Santa Clara, CA, USA). The c DNA synthesis products were used in an *in vitro* transcription reaction containing T7 RNA polymerase and biotinylated nucleotide analog (pseudouridine base). The labeled cRNA products were then fragmented, loaded on to the GeneChip(R) Human Genome U133 Plus2.0 array (Affymetrix Japan K. K) and hybridized according to the manufacturer's protocol. Streptavidin-phycoerythrin (Molecular Probe) was used as the fluorescent conjugate to detect hybridized target sequences. Raw intensity data from the GeneChip array were analyzed with GeneChip Operating Software (Affymetrix Japan K. K).

2.9 Real-time RT-PCR

For the quantification of ST6Gal1 in GIST tissues, we employed the real time RT-PCR method. Total RNA were prepared from surgical samples of GIST with the RNeasy Kit (Qiagen, Valencia, CA) method and cDNA were synthesized by using the Kit. A standard curve for ST6Gal1 was generated by the serial dilution of a plasmid vector DNA containing the ST6Gal1 gene. The primer sequences for ST6Gal1 were: forward primer, 5'-gcctgatgaactctcagttggttac-3'; reverse primer, 5'-agatgggtcccatacaattaggatt-3'.Primers and cDNA were the added to SYBR pre-mix (Invitrogen), which contained all reagents required for PCR. The PCR conditions consisted of 1 cycle at 98°C for 5 min and 45 cycles at 98°C for 10 s, 55°C for30 s, and 72°C for 30 s. PCR products were measured continuously with the My IQ™ Single-Color Real-Time PCR Detection System (Bio-Rad).

3 Results

H&E staining and immunohistochemistry for KIT and CD34 identified seven mesenchymal tumors as GIST (Table 1), all of which were positive for KIT and CD34. There were three male and four female patients with a median age of 18 years (range: 10–28) at the time of diagnosis. Six of the tumors

Table 1. Summary of clinical characteristics of juvenile gastrointestinal stromal tumors examined in this study

Case	Age	Sex	Locus	Tumor size (cm)	Mitotic count (/50HPF)	Immunohistochemistry		Mutation
						KIT	CD34	
J1	10	M	Gastric	5.5	1	+	+	No mutation
J2	16	F	Small intestine	10	5	+	+	KIT exon11
J3	18	M	Gastric	4.5	1	+	+	No mutation
J4	18	M	Gastric	7	5	+	+	No mutation
J5	23	F	Gastric	5.5	0	+	+	KIT exon11
J6	26	F	Gastric	6.5	0	+	+	No mutation
J7	28	F	Gastric	1.5	0	+	+	KIT exon11

were located in the stomach and one in the small intestine. Mutational analysis using PCR and DNA sequencing was performed for *KIT* and *PDGFRA*, and *KIT* mutations were detected at exon 11 in three cases, while no *KIT* or *PDGFRA* mutation could be detected in the other four tumors. The control group comprised seven adult GIST (*KIT* mutations were detected at exon11 in five cases, *PDGFRA* mutation at exon 12 was detected in one case and no mutation in either *KIT* or *PDGFRA* was detected in one case).

To explore other RTK oncoproteins that might participate in GIST pathogenesis, we performed immunoprecipitation (IP) with an anti-phosphotyrosine kinase antibody. Phosphotyrosine immunoblotting of these IP products from juvenile GIST (GISTJ3, 4, 6) identified a phosphorylated protein of about 135 kDa (Fig. 1), which was slightly below the band of phosphorylated KIT (145 kDa). To identify this phosphorylated protein, we excised this silver-stained band visualized only in juvenile GIST with Western blotting (Fig. 2A). Next, this protein band was digested with trypsin and the extracted peptides were analyzed with LC-MS/MS. The spectra thus acquired were searched against the Swiss-Prot database with the aid of the MASCOT search engine. In this manner, KIT could be identified as the specific phosphorylated protein (Table 2). We confirmed the expression of phosphorylated KIT by means of Western blotting using a commercially available anti-phosphotyrosine mAb and anti-KIT polyclonal antibody (Fig. 2B). We found that juvenile GIST also expressed phosphorylated KIT but at a different level from that observed in the adult controls. However, adult wild-*KIT* GIST expressed the same level of KIT band as that in control.

To determine whether this phosphorylated KIT in juvenile GIST is functional, we examined the downstream signals of KIT and compared the signal transduction pathways activated in juvenile GIST with those in adult *KIT* mutant GIST. Juvenile GIST showed uniform activation of signaling intermediates protein kinase B (AKT), mitogen-activated protein kinase (MAPK), and STAT (signal transducers and activators of transcription) proteins Stat1 and Stat3, and all three were activated in most *KIT* mutant GIST (Fig. 2C). Moreover, the juvenile GIST lacked expression of phospho-

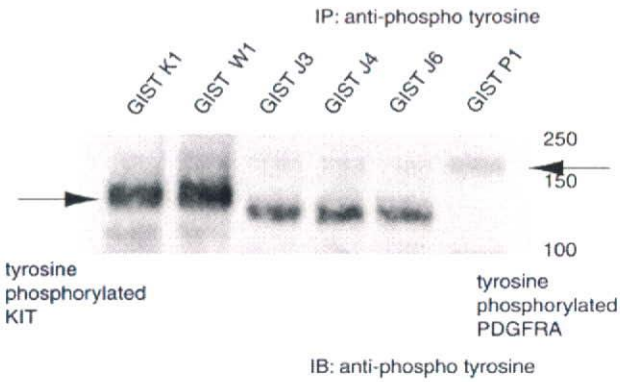

Figure 1. Identification of phosphorylated receptor tyrosine kinases in adult and juvenile GIST (GIST K: KIT exon 11 mutant-type; GIST W: adult *KIT* and *PDGFRA* wild type; GIST J: juvenile *KIT* and *PDGFRA* wild type; GIST P-1: *PDGFRA* exon12 mutant-type) Western blot analysis of anti-tyrosine phosphorylated proteins in GIST samples. GIST K showed tyrosine phosphorylated KIT and GIST P showed tyrosine phosphorylated PDGFRA. GIST P showed an unknown phosphorylated protein about 135 kDa.

Stat5, despite strong expression of total Stat5, which is also typical of adult *KIT* mutant GIST. These findings suggest that this phosphorylated KIT in juvenile GIST is also activated and acts as a key protein.

We speculated that the difference in the apparent molecular weight (kDa) of KIT protein bands between adult and juvenile GIST might be caused by a PTM. PTM refers to the chemical modification of a protein after its translation. After translation, PTM of amino acids extends the range of functions of the protein by attaching to it other biochemical functional groups such as acetates, phosphates, various lipids and carbohydrates. First, we examined the glycosylation of KIT. To eliminate the glycosylation of N-glycans after the addition of glycopeptidase F to the samples and incubation for several hours, we used western blotting and found that each KIT band had shifted down about 25 kDa lower and equaled at the same level (Fig. 3A). This suggests that the glycosylation of N-glycans was the cause of this change. Furthermore, we performed Western blotting after adding neur-

Table 2. Result of LC-MS/MS and database searching for protein identification[a)]

Observed	Mr(expt)	Mr(calc)	Delta	Miss	Score	Expect	Residue matched	Peptide sequence
551.37	550.36	550.31	0.05	0	30	0.038	589 – 593	R.LSFGK.T
497.02	992.02	991.50	0.52	0	42	0.01	614 – 623	K.SDAAMTVAVK.M
524.57	1047.12	1046.57	0.55	0	77	0.000003	272 – 281	R.QATLTISSAR.V
559.51	1117.01	1116.59	0.42	0	62	0.0001	373 – 381	R.YVSELHLTR.L
575.53	1149.04	1148.59	0.45	0	35	0.047	56 – 65	R.LLCTDPGFVK.W
642.03	1282.05	1281.69	0.37	0	47	0.0022	624 – 634	K.MLKPSAHLTER.E
691.07	1380.12	1379.73	0.39	0	73	0.000006	472 – 484	K.LVVQSSIDSSAFK.H
723.49	1444.97	1444.64	0.33	0	44	0.0053	182 – 193	R.LCLHCSVDQEGK.S
819.60	1637.18	1635.78	1.40	0	50	0.0012	136 – 149	R.CPLTDPEVTNYSLK.G
932.52	1863.03	1861.84	1.19	0	39	0.013	889 – 904	R.MLSPEHAPAEMYDIMK.T

a) KIT_HUMAN Mass: 111163 Score: 528 Queries matched: 11. Mast/stem cell growth factor receptor precursor (EC 2.7.10.1) (SCFR) (Proto-oncogene tyrosine kinase).

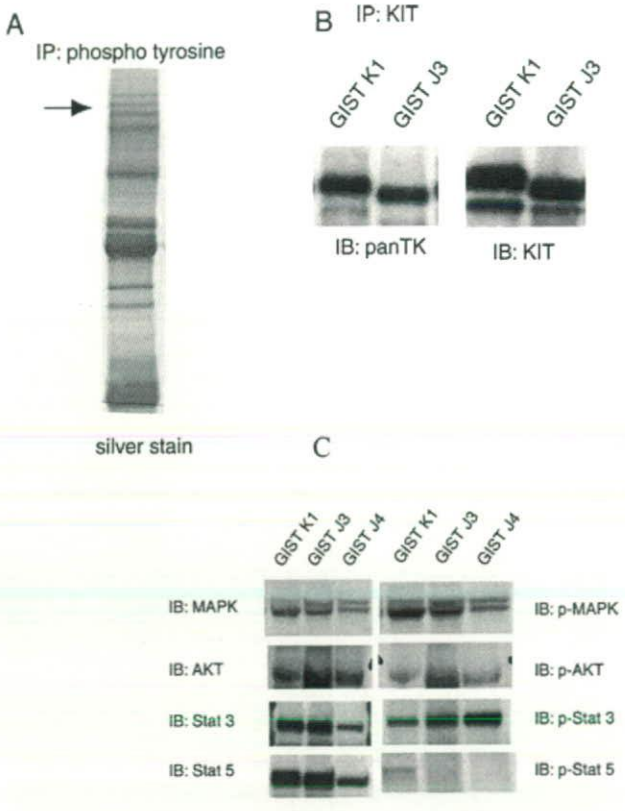

Figure 2. (A) Silver staining of anti-KIT immunoprecipitation product for juvenile GIST. Positive band of about 130 kDa (arrow) identified by Western blotting was excised for mass spectrometer. (B) Western blotting analysis of anti-KIT immunoprecipitation product for adult and juvenile GIST. Phosphorylated KIT bands were visualized in both GIST at different levels. (C) Cell signaling profiles of juvenile GIST and adult KIT-mutant GIST. Whole-cell lysates were prepared from frozen samples and immunoblots were detected with antibodies to phosphorylated and total form of AKT, MAPK, and Stats. All GIST expressed phosphorylated AKT, MAPK, Stat1, and Stat3, whereas Stat 5 was not tyrosine-phosphorylated.

aminidase and found that each KIT band shifted down about 15 kDa lower and equaled at the same level (Fig. 3B), suggesting that this difference is also caused by the modification of sialic acid.

Sialyltransferase is an enzyme, which regulates sialylation, and the alteration of transferase activity in human cancers has been demonstrated [22–24]. We therefore performed the DNA-microarray to investigate sialyltransferase expression in adult GIST and juvenile GIST. The DNA-microarray consisted of more than 47 000 genes, including all known human sialyltransferases. Table 3 shows 17 sialyltransferase genes, three of which were reduced significantly. We focused on ST6Gal1 gene expression in GIST tissues because it is related to sialylation for the synthesis of N-glycans. We performed real-time RT-PCR using four adult GIST tissues and three juvenile GIST tissues and found that ST6Gal1 gene expression in juvenile GIST was significantly weaker than that in adult GIST (Fig. 4A).

To examine the influence of the decline of ST6Gal1 in juvenile GIST tissues, we investigated levels of α2-6 sialylation on KIT. SSA-lectin precipitation, followed by KIT immunoblotting showed a dramatic decrease in α2-6 sialylation on KIT was observed in juvenile GIST, compared to that in adult GIST (Fig. 4B). Therefore, the down-regulation of ST6Gal1 expression resulted in the decline of addition of α2-6 sialic acids residues to KIT.

Our investigation of juvenile GIST showed activation of KIT, which showed a lower molecular weight than in adult GIST. It is possible that this difference is caused by PTM such as the sialylation of N-glycan. In addition, it is suggested that this difference is involved in the activation of KIT.

4 Discussion

Juvenile GIST usually express KIT, but have no mutations in the *KIT* and *PDGFRA* genes, which are thought to be involved in the pathogenesis for GIST [1, 2, 9, 10], so that it

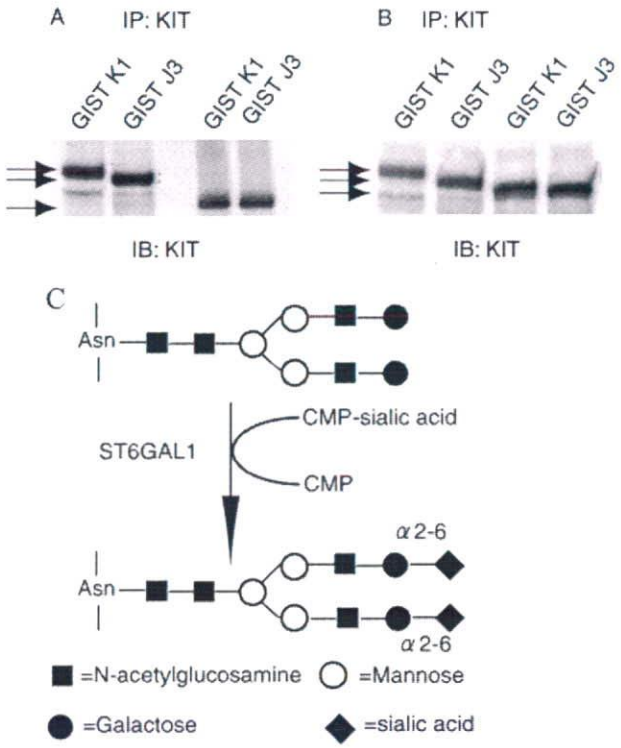

Figure 3. (A) Western blotting analysis of anti-KIT immunoprecipitation product for adult and juvenile GIST, before (right) and after (left) treated with glycopeptidase F to cleave N-glycans, showing that each KIT band has shifted about 25 kDa lower and equaled at the same level. (B) Western blotting analysis of anti-KIT immunoprecipitation product for adult and juvenile GIST, before (right) and after (left) treated with neuraminidase to cleave sialic acid, showing that each KIT band has shifted about 15 kDa lower and equaled at the same level. (C) Reaction pathway for the biosynthesis of N-glycans by ST6Gal1.

was assumed that these juvenile GIST had another pathway of multiplication. Because both *KIT* and *PDGFRA*, known as key proteins, belong to the RTK protein family, we focused our investigation on this family. After Western blotting of tyrosine phosphorylated protein, a specific band was visualized which was below the normal phosphorylated KIT band and identified by spectrometry as KIT. Furthermore, we were able to prove that this KIT was also activated and that juvenile GIST featured the same downstream signal pathways. These findings led us to think that this aberrant KIT could be a key to the pathogenesis of juvenile GIST. Furthermore, since adult GIST with neither mutation show the same molecular weight as other adult GIST, juvenile GIST must have a specific pathogenesis.

To identify the reason for this difference, we examined various post-translational modifications, such as phosphorylation, proteinase, and glycosylation. The result indicated that this difference was due to a difference in the modification of N-glycans. The glycosylation of N-glycans represents a critically important PTM reaction, so that a comprehensive

Table 3. Differentially expressed genes of Sialyltransferase by DNA microarray

Gene symbol	Expression up or down	Fold	*p*-value
ST3Gal1	up	2.0839	0.0523
ST3Gal2	down	2.5711	0.0040*
ST3Gal3	down	1.2836	0.1731
ST3Gal4	down	2.7604	0.1184
ST3Gal5	down	1.451	0.3697
ST3Gal6	up	1.3889	0.7047
ST6Gal1	down	2.7511	0.0011*
ST6Gal2	up	4.4912	0.1847
ST6GalNac3	up	2.1602	0.1147
ST6GalNAC4	down	2.3451	0.0054*
ST8Sia1	up	2.8927	0.2723
ST8Sia4	down	4.2777	0.0828
SiaT4A	down	1.5886	0.0731
SiaT4B	down	1.6657	0.0968
SiaT6	up	1.4954	0.1647
SiaT7B	up	1.3539	0.1544
SiaT7E	down	2.0347	0.2652
SiaT8C	down	1.329	0.7275

* $p < 0.01$

functional analysis of proteins qualifies as a target for the next stage of proteomic research. It is a common knowledge that over 50% of mammalian serum proteins and about 80% of cell membrane proteins are glycosylated and that glycans perform crucial functions in various biological events including cell recognition [25], adhesion [26], and cell-cell interaction [27]. Glycans of glycoproteins, which are displayed on cell surface membranes, change structurally during carcinogenesis and development [28]. For example, the sugar chain in the epidermal growth factor receptor (EGFR), which also belongs to the RTK family (type III) and has a similar 3D to that of KIT, is reportedly crucial for EGF binding and the prevention of spontaneous oligomerization of the EGFR, which may otherwise lead to uncontrollable receptor activation [29, 30]. For this reason, we hypothesized that this aberrant expression of glycosylation of KIT in juvenile GIST was essential for changing KIT to its activated form. Since KIT contains 11 potential sites for N-glycosylation, we prepared several N-glycosylation mutants of KIT (Asn→Gln) to clarify whether a sugar chain is important or essential for receptor functions such as ligand binding and dimerization regulation. We also transfected several N-glycosylation mutants of KIT to various cell lines, such as HEK293, HepG2, and NUGC3 (data not shown). However, we could not obtain the same result as that reported for the EGFR. Although the KIT protein band was visualized, no gap between normal KIT and mutated KIT was apparent and KIT was not phosphorylated. We therefore concluded that the gap was not attributable to one site of N-glycans change only. Moreover, it was

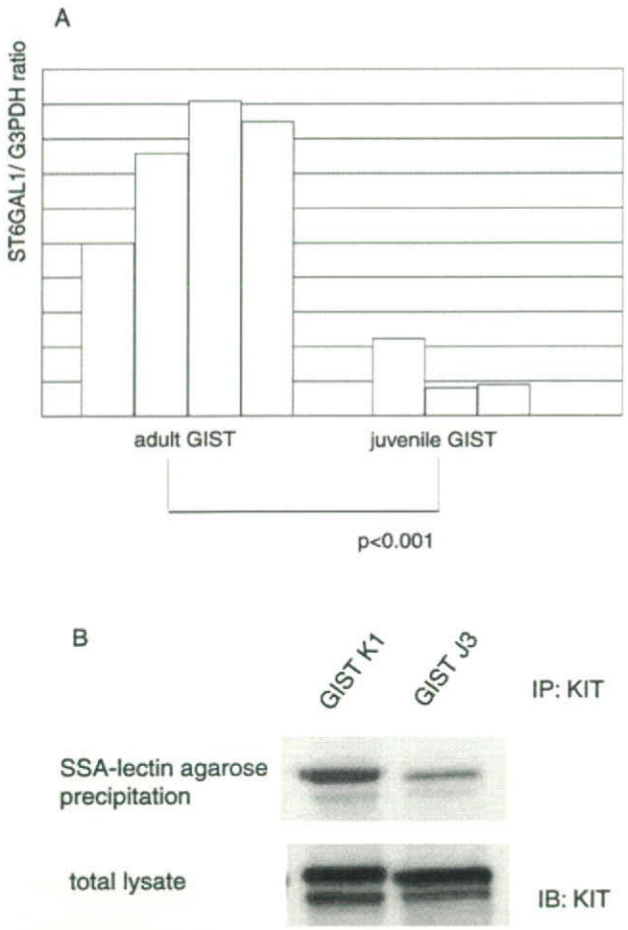

Figure 4. (A) Quantitative real-time PCR analyses of ST6Gal1 in adult and juvenile GIST. The relative amount of ST6Gal1 was normalized to the amount of the G3PDH transcript. Data were obtained by four adult and three juvenile GIST samples from triplicate experiments. The expression of ST6Gal1 in juvenile GIST tissues was significantly lower than that in adult GIST. (B) Western blotting analysis of SSA-lectin agarose precipitation for adult and juvenile GIST. The amount of the KIT protein obtained from juvenile GIST was significantly smaller than that of adult GIST.

suspected that conditions including cell type and N-glycosylation might not be the same *in vitro* as *in vivo* and therefore not a good model.

Next, we examined the KIT band after treating it with neuraminidase. In both GIST groups, the KIT band moved slightly to the same level, thus reducing the gap. This means that sialic acid as well as N-glycans is involved with the gap. To identify the reason for the change in the modification of sialic acid, we used a DNA microarray, which showed that three sialyl-transferases were significantly reduced, and we focused on ST6Gal1 because it is involved in N-glycans synthesis. Real time RT-PCR showed that the level of ST6Gal1 was significantly lower in juvenile GIST tissues than in adult GIST tissues. In addition, in the protein level, addition of α2-6 sialic acids to KIT was decreased in juvenile GIST, compared to adult GIST.

ST6Gal1 is a highly typical enzyme, which transfers Neu5Ac residues in α2-6 linkage to Galβ1-4GlcNAc units on N-glycans (Fig. 3C) [31, 32]. Several malignancies, including colon carcinoma [33–35], and breast carcinoma [36], acute myeloid leukemia [37], cervical carcinoma [38] and some types of brain tumors [39] show an elevation of ST6Gal1 activity or of the transcript. Use of the α2-6-sialyl-specific lectins from *Sambucus nigra* (SNA) [40] and *Tricosanthes japonica* as probes, has demonstrated a marked increase in the degree of α2-6 sialylation in colon cancer tissues [41]. Using transfection with the antisense RNA, we tried to move the ST6Gal1 of the H187 down, which originates from a lung small cell carcinoma and has the expression of KIT. However, neither movement nor phosphorylation of the KIT protein band was observed. H187 expresses KIT, but is not concerned with pathogenesis. Since this subset of juvenile GIST is very rare and its cell line has not been the subject of any reports, we could not establish an appropriate model, although we feel it deserves to be established and researched in more detail. Furthermore, we used mice with the ST6Gal1 gene knocked out, which reportedly display only immunological alterations [42]. However, their KIT expressing mast cells are otherwise normal (data not shown). The human type KIT protein is different from the murine type, especially in terms of the extracellular domain, so that KIT may not be activated in the former.

While decreases in sialylation level on KIT seem to be a cause of juvenile GIST, no direct evidence that de-sialylation increases KIT signaling has been shown. Previous reports showed cellular sialylation could control a signaling of CD95 (APO-1/Fas) -mediated apoptosis [43, 44]. These reports suggested that cell surface sialylation could inhibit binding of Fas-ligand to the receptor because of negative charge of the oligosaccharides. Therefore, de-sialylation of KIT might promote the binding capacity to its ligand. Recently, it was reported that N-glycan branching of EGF-R regulates its signaling through galectin 3 [45]. β1-6 GlcNAc branching on EGF-R has polylactosamine structures, resulting in control of endocytosis of EGF-R. Furthermore, metabolic regulation of cellular transition between growth and arrest could control N-glycan branching structures in complicated pathway [46]. Siglec, which belongs to a family of lectin, recognize α2-6 Sialylation and involves in immune system [47]. Similar relationship between polylatosamine and galectin 3 on EGF-R could be observed in cases of sialylation and lectins of a siglec family on KIT. In such cases, endocytosis of KIT might be increased with de-sialylation, resulting in up-regulation of KIT signaling.

In conclusion, we discovered aberrant glycosylation of KIT in juvenile GIST, and we believe that this difference may contribute in the progression of juvenile GIST.

The authors are grateful for the helpful comments from Dr. Shinobu Hashizume and Dr. Yasuhiro Hashimoto, Glyco-chain Functions Laboratory, the Institute of Physical and Chemical

Research, RIKEN. This work was supported in part by Grants-Aids for Scientific Research from the Japanese Ministry of Education, Science, Culture and Sports.

The authors have declared no conflict of interest.

5 References

[1] Hirota, S., Isozaki, K., Moriyama, Y., Hashimoto, K. *et al.*, Gain-of-function mutations of c-kit in human gastrointestinal stromal tumors. *Science* 1998, *279*, 577–580.

[2] Fishman, A. P., Rosai, J. (Eds.), Gastrointestinal tract. In: *Ackerman's Surgical Pathology*, Mosby, St Louis 1996, 8th edn., pp.645–647.

[3] Kindoblom, L., Remotti, H., Aldenborg, F., Meis-Kindblom, J. M., Gastrointestinal pacemaker cell tumor (GIPACT): gastrointestinal tumors show phenotypic characteristics of the interstitial cells of Cajar. *Am. J. Pathol.* 1998, *152*, 1259–1269.

[4] Taniguchi, M., Nishida, T., Hirota, S., Isozaki, K. *et al.*, Effect of c-kit mutation on prognosis of gastrointestinal stromal tumors. *Cancer Res.* 1999, *59*, 4297–4300.

[5] Lasota, J., Jasinski, M., Sarlomo-Rikala, M., Miettinen, M., Mutations in exon 11 of c-kit occur preferentially in malignant versus benign gastrointestinal stromal tumors and do not occur in leiomyomas or leiomyosarcomas. *Am. J. Pathol.* 1999, *154*, 53–60.

[6] Nishida, T., Hirota, S., Taniguchi, M., Hashimoto, K. *et al.*, Familial gastrointestinal stromal tumours with germline mutation of the kit gene. *Nat. Genet.* 1998, *19*, 323–324.

[7] Hirota, S., Nishida, T., Isozaki, K., Taniguchi, M. *et al.*, Familial gastrointestinal stromal tumors associated with dysphagia and novel type germline mutation of KIT gene. *Gastroenterology* 2002, *122*, 1493–1499.

[8] Isozaki, K., Terris, B., Belghiti, J., Schiffmann, S. *et al.*, Germline-activating mutation in the kinase domain of KIT gene in familial gastrointestinal stromal tumors. *Am. J. Pathol.* 2000, *157*, 1581–1585.

[9] Heinrich, M. C., Corless, C. L., Duensing, A., McGreevey, L. *et al.*, PDGFRA activating mutations in gastrointestinal stromal tumors. *Science* 2003, *299*, 708–710.

[10] Hirota, S., Ohashi, A., Nishida, T., Isozaki, A. *et al.*, Gain-of-function mutation of platelet-derived growth factor receptor αgene in gastrtointestinal stromal tumors. *Gastroenterology* 2003, *125*, 660–667.

[11] Kinoshita, K., Hirota, S., Isozaki, K., Ohashi, A. *et al.*, Absence of c-kit gene mutations in gastrointestinal stromal tumours from neurofibromatosis type 1 patients. *J. Pathol.* 2004, *202*, 80–85.

[12] Carney, J. A., Sheps, S. G., Go, V. L., Gordon, H., The triad of gastric leiomyosarcoma, functioning extra-adrenal paraganglioma and pulmonary chondroma. *Cancer* 1979, *43*, 374–382.

[13] Diment, J., Tamborini, E., Casali, P., Gronchi, A. *et al.*, Carney triad: case report and molecular analysis of gastric tumor. *Hum. Pathol.* 2005, *36*, 112–116.

[14] Prakash, S., Sarran, L., Socci, N., DeMatteo, R P. *et al.*, Gastrointestinal stromal tumors in children and young adults: a clinicopathologic, molecular, and genomic study of 15 cases and review of the literature. *J. Pediatr. Hematol. Oncol.* 2005, *7*, 179–187.

[15] Miettinen, M., Lasota, J., Sobin, L H., Gastrointestinal stromal tumors of the stomach in children and young adults: a clinicopathologic, immunohistochemical, and molecular genetic study of 44 cases with long-term follow-up and review of the literature. *Am. J. Surg. Pathol.* 2005, *29*, 1373–1381.

[16] O'Sullivan, M. J., McCabe, A., Gillett, P., Penman, I. D. *et al.*, Multiple gastric stromal tumors in a child without syndromic association lacks common KIT or PDGFRalpha mutations. *Pediatr. Dev. Pathol.* 2005, *8*, 685–689.

[17] Hayashi, Y., Okazaki, T., Yamataka, A., Yanai, T. *et al.*, Gastrointestinal stromal tumor in a child and review of the literature. *Pediatr. Surg. Int.* 2005, *21*, 914–917.

[18] DeMatteo, R. P., Lewis, J. J., Leung, D., Mudan, S. S. *et al.*, Two hundred gastrointestinal stromal tumors: recurrence patterns and prognostic factors for survival. *Ann. Surg.* 2000, *231*, 51–58.

[19] Kerr, J. Z., Hicks, M. J., Nuchtern, J. G., Saldivar, V. et. al., Gastrointestinal autonomic nerve tumors in the pediatric population: a report of four cases and a review of the literature. *Cancer* 1999, *85*, 220–230.

[20] Hirota, S., Ito, A., Nagoshi, J., Takeda, M. *et al.*, Expression of bone matrix protein messenger ribonucleic acids in human breast cancers. Possible involvement of osteopontin in development of calcifying foci. *Lab. Invest.* 1995, *72*, 64–69.

[21] Shevchenko, A., Wilm, M., Vorm, O., Mann, M., Mass spectrometric sequencing of proteins silver-stained polyacrylamide gels. *Anal. Chem.* 1996, *68*, 850–858.

[22] Hedlund, M., Ng, E., Varki, A., Varki, N. M., Alpha 2-6 linked sialic acids on N-glycans modulate carcinoma differentiation *in vivo*. *Cancer Res.* 2008, *68*, 388–394.

[23] Senda, M., Ito, A., Tsuchida, A., Hagiwara, T. *et al.*, Identification and expression of a sialyltransferase responsible for the synthesis of disialylgalactosylgloboside in normal and malignant kidney cells: downregulation of ST6GalNAc 2165; in renal cancers. *Biochem. J.* 2007, *402*, 459–470.

[24] Schneider, F., Kemmner, W., Haensch, W., Franke, G. *et al.*, Overexpression of sialyltransferase CMP-sialic acid:Galbeta 1,3GalNAc-R alpha 6-sialyltransferase is related to poor patient survival in human colorectal carcinoma. *Cancer Res.* 2001, *61*, 4605–4611.

[25] Varki, A., Biological roles of oligosaccharides: all of the theories are correct. *Glycobiology* 1993, *3*, 97–130.

[26] Isaji, T., Gu, J., Nishiuchi, R., Zhao, Y. *et al.*, Introduction of bisecting GlcNAc into integrin alpha5beta1 reduces ligand binding and down-regulates cell adhesion and cell migration. *J. Biol. Chem.* 2004, *279*, 19747–19754.

[27] Stanley, P. Biological consequences of overexpressing or eliminating N-acetylglucosaminyltransferase-TIII in the mouse. *Biochim. Biophys. Acta* 2002, *1573*, 363–368.

[28] Hakomori, S., Aberrant glycosylation in tumors and tumor-associated carbohydrate antigens. *Adv. Cancer Res.* 1989, *52*, 257–331.

[29] Tsuda, T., Ikeda, Y., Taniguchi, N., The Asn-420-linked sugar chain in human epidermal growth factor receptor suppresses ligand-independent spontaneous oligomerization. Possible role of a specific sugar chain in controllable receptor activation. *J. Biol. Chem.* 2000, *275*, 21988–21994.

[30] Yu, X., Sharma, K. D., Takahashi, T., Iwamoto, R. *et al.*, Ligand-independent dimer formation of epidermal growth factor receptor (EGFR) is a step separable from ligand-induced EGFR signaling. *Mol. Biol. Cell* 2002, *13*, 2547–2557.

[31] Weinstein, J., de Souza-e-Silva, U., Paulson, J. C., Purification of a Gal beta 1 to 4GlcNAc alpha 2 to 6 sialyltransferase and a Gal beta 1 to 3(4)GlcNAc alpha 2 to 3 sialyltransferase to homogeneity from rat liver. *J. Biol. Chem.* 1982, *257*, 13835–13844.

[32] Weinstein, J., de Souza-e-Silva, U., Paulson, J. C., Sialylation of glycoprotein oligosaccharides N-linked to asparagine. Enzymatic characterization of a Gal beta 1 to 3(4)GlcNAc alpha 2 to 3 sialyltransferase and a Gal beta 1 to 4GlcNAc alpha 2 to 6 sialyltransferase from rat liver. *J. Biol. Chem.* 1982, *257*, 13845–13853.

[33] Dall'Olio, F., Malagolini, N., di Stefano, G., Minni, F. *et al.*, Increased CMP-NeuAc:Gal beta 1,4GlcNAc-R alpha 2,6 sialyltransferase activity in human colorectal cancer tissues. *Int. J. Cancer* 1989, *44*, 434–439.

[34] Dall'Olio, F., Malagolini, N., Serafini-Cessi, F., Enhanced CMP-NeuAc:Gal beta 1,4GlcNAc-R alpha 2,6 sialyltransferase activity of human colon cancer xenografts in athymic nude mice and of xenograft-derived cell lines. *Int. J. Cancer* 1992, *50*, 325–330.

[35] Gessner, P., Riedl, S., Quentmaier, A., Kemmner, W., Enhanced activity of CMP-neuAc:Gal beta 1-4GlcNAc:alpha 2,6-sialyltransferase in metastasizing human colorectal tumor tissue and serum of tumor patients. *Cancer Lett.* 1993, *75*, 143–149.

[36] Recchi, M. A., Hebbar, M., Hornez, L., Harduin-Lepers, A. *et al.*, Multiplex reverse transcription polymerase chain reaction assessment of sialyltransferase expression in human breast cancer. *Cancer Res.* 1998, *58*, 4066–4070.

[37] Skacel, P. O., Edwards, A. J., Harrison, C. T., Watkins, W. M., Enzymic control of the expression of the X determinant (CD15) in human myeloid cells during maturation: the regulatory role of 6-sialytransferase. *Blood* 1991, *78*, 1452–1460.

[38] Wang, P. H., Li, Y. F., Juang, C. M., Lee, Y. R. *et al.*, Altered mRNA expression of sialyltransferase in squamous cell carcinomas of the cervix. *Gynecol. Oncol.* 2001, *83*, 121–127.

[39] Kaneko, Y., Yamamoto, H., Kersey, D. S., Colley, K. J. *et al.*, The expression of Gal beta 1,4GlcNAc alpha 2,6 sialyltransferase and alpha 2,6-linked sialoglycoconjugates in human brain tumors. *Acta Neuropathol. (Berl)* 1996, *91*, 284–292.

[40] Shibuya, N., Goldstein, I. J., Broekaert, W. F., Nsimba-Lubaki, M. *et al.*, The elderberry (*Sambucus nigra* L.) bark lectin recognizes the Neu5Ac(alpha 2-6)Gal/GalNAc sequence. *J. Biol. Chem.* 1987, *262*, 1596–1601.

[41] Yamashita, K., Fukushima, K., Sakiyama, T., Murata, F. *et al.*, Expression of Sia alpha 2–>6Gal beta 1–>4GlcNAc residues on sugar chains of glycoproteins including carcinoembryonic antigens in human colon adenocarcinoma: applications of *Trichosanthes japonica* agglutinin I for early diagnosis. *Cancer Res.* 1995, *55*, 1675–1679.

[42] Hennet, T., Chui, D., Paulson, J. C., Marth, J. D., Immune regulation by the ST6Gal sialyltransferase. *Proc. Natl. Acad. Sci. USA* 1998, *95*, 4504–4509.

[43] Peter, M. E., Hellbardt, S., Schwartz-Albiez, R., Westendorp, Mo. *et al.*, Cell surface sialylation plays a role in modulating sensitivity towards APO-1-mediated apoptotic cell death. *Cell Death Differ.* 1995, *2*, 163–171.

[44] Keppler, O. T., Peter, M. E., Hinderlich, S., Moldenhauer, G. *et al.*, Differential sialylation of cell surface glycoconjugates in a human B lymphoma cell line regulates susceptibility for CD95 (APO-1/Fas)-mediated apoptosis and for infection by a lymphotropic virus. *Glycobiology* 1999, *9*, 557–569.

[45] Lajoie, P., Partridge, E. A., Guay, G., Goetz, J. G. *et al.*, Plasma membrane domain organization regulates EGFR signaling in tumor cells. *J. Cell Biol.* 2007, *179*, 341–356.

[46] Lau, K. S., Partridge, E. A., Grigorian, A., Silvescu, C. I. *et al.*, Complex N-glycan number and degree of branching cooperate to regulate cell proliferation and differentiation. *Cell* 2007, *129*, 123–134.

[47] Crocker, P. R., Siglecs: sialic-acid-binding immunoglobulin-like lectins in cell-cell interactions and signaling. *Curr. Opin. Struct. Biol.* 2002, *12*, 609–615.

Protein Expression and Purification 61 (2008) 78–82

Contents lists available at ScienceDirect

Protein Expression and Purification

journal homepage: www.elsevier.com/locate/yprep

Ligand-independent assembly of purified soluble magic roundabout (Robo4), a tumor-specific endothelial marker

Mai Yoshikawa [a], Yohei Mukai [a,*], Yoshiaki Okada [a], Yasuo Yoshioka [b], Shin-ichi Tsunoda [c], Yasuo Tsutsumi [a,c], Naoki Okada [a], William C. Aird [d], Takefumi Doi [a], Shinsaku Nakagawa [a,*]

[a] Department of Biotechnology and Therapeutics, Graduate School of Pharmaceutical Sciences, Osaka University, 1-6 Yamadaoka, Suita, Osaka 565-0871, Japan
[b] The Center for Advanced Medical Engineering and Informatics, Osaka University, 1-6 Yamadaoka, Suita, Osaka 565-0871, Japan
[c] Laboratory of Pharmaceutical Proteomics, National Institute of Biomedical Innovation (NiBio), 7-6-8 Asagi, Saito, Ibaraki, Osaka 567-0085, Japan
[d] Center for Vascular Biology Research and Division of Molecular and Vascular Medicine, Beth Israel Deaconess Medical Center, Harvard Medical School, Boston, MA 02215, USA

ARTICLE INFO

Article history:
Received 21 March 2008
and in revised form 1 May 2008
Available online 61x

Keywords:
Magic roundabout
Robo4
Angiogenesis
Vessel marker
Multimer

ABSTRACT

Magic roundabout (Robo4) is the fourth recently identified member of the roundabout receptor family. Robo4 is predominantly expressed in embryonic or tumor vascular endothelium and is considered important for vascular development and as a candidate tumor endothelial marker. Much remains unknown about the Robo4 molecule, however, such as its ligands, structure, and the details of its function. Thus, we aimed to establish an expression and purification method for obtaining soluble recombinant human Robo4 (shRobo4) and mouse Robo4 (smRobo4) for use in Robo4 characterization studies. In this work, we expressed the extracellular domain of hRobo4 and mRobo4 in mammalian 293F cells and purified them by two-step chromatography. Based on gel-filtration chromatography and Blue Native polyacrylamide gel electrophoresis, these purified proteins exist as multimers. The shRobo4 and smRobo4 we obtained will be useful in advanced studies to determine the importance of multimerization, identify the ligands, and elucidate the ligand–receptor interactions and Robo4-mediated signaling. The results of these studies will help to elucidate the role of Robo4 in angiogenesis and perhaps eventually contribute to the development of novel vessel-targeting therapies.

Magic roundabout (Robo4)[1] is the fourth recently identified member of the roundabout receptor family [1,2]. Robo1–3 are highly expressed in the nervous system and regulate axon guidance, neural migration, and leukocyte chemotaxis [3–5]. The specificity of Robo4 expression, however, is unique compared with the other three members [2]; it is highly expressed in embryonic vasculature and endothelium, but not in the nervous system [6]. Robo4 also has a different structural repeat sequence (Fig. 1). The extracellular domain of Robo4, comprising the ligand-binding domain, includes only two immunoglobulin (Ig) domains and two fibronectin domains, whereas the extracellular domains of the other Robo family members include five Ig domains and three fibronectin domains. Further, in the cytoplasmic region, which usually consists of four conserved domains (CC0, CC1, CC2, and CC3), Robo4 has only two, CC0 and CC2 [2,7]. Thus, Robo4 has unique physical characteristics compared with the other Robos.

Robo4 induces endothelial migration and regulates angiogenesis [2,5,8–10]. Some reports suggest that Robo4 is highly expressed in tumors compared to normal tissue, and is expressed exclusively in tumor neovascular endothelium [2,8,11], thus because of its expression pattern Robo4 may act as a tumor-specific endothelial marker. Robo4 is expected to be widely applicable as a specific marker for cancer diagnosis and as a therapeutic molecule.

The precise function of Robo4 remains unclear, however, because it was identified only recently. In fact, Robo4 does not bind to Slit2, a common ligand of Robo1–3 [12–14], and its ligands remain unknown [7,15]. Moreover, although Rho GTPase activation induces Robo signaling, the trigger factor for Robo4 is unknown [16]. While it is reported that the self-assembly of Robo4 may influence its signal initiation [16], this has not yet been established. The identification of ligands for Robo4 and multimerization analysis may provide clues to Robo signaling and function.

Here, we aimed to establish an expression and purification method for soluble recombinant human Robo4 (shRobo4) and mouse Robo4 (smRobo4) to facilitate basic studies of Robo4 and enable further approaches for the development of new therapies. We then used our purified shRobo4 and smRobo4 to analyze

* Corresponding authors. Fax: +81 6 6879 8179.
E-mail addresses: yohe@phs.osaka-u.ac.jp (Y. Mukai), nakagawa@phs.osaka-u.ac.jp (S. Nakagawa).

[1] *Abbreviations used:* Robo4, magic roundabout; Ig, immunoglobulin; PCR, polymerase chain reaction; SDS–PAGE, sodium dodecyl sulfate–polyacrylamide gel electrophoresis; Ni–NTA, nickel–nitrilotriacetic acid; ECD, extracellular domain; FN, fibronectin domain; TM, transmembrane domain; ICD, intracellular domain; ss, signal sequence.

1046-5928/$ - see front matter © 2008 Elsevier Inc. All rights reserved.
doi:10.1016/j.pep.2008.05.006

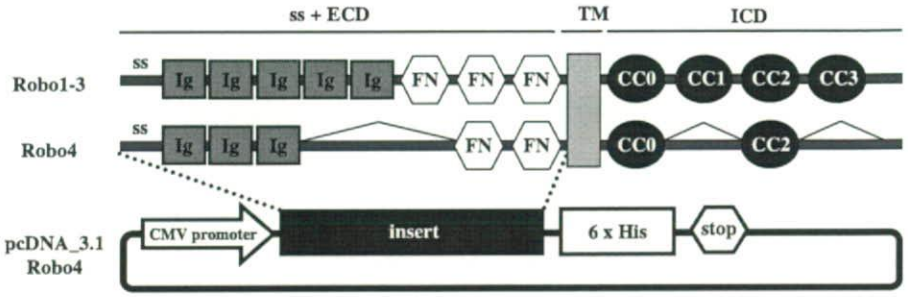

Fig. 1. Schematic representation of the Robo family and construction of the Robo4 expression vector. Robo4 has an extracellular domain (ECD) comprising three immunoglobulin (Ig) domains and two fibronectin domains (FNs), a transmembrane domain (TM), and an intracellular domain (ICD) with two conserved motifs (CC0 and CC2). On the other hand, the extracellular domain of Robo1–3 comprises five Igs, three FNs, and four CCs. The expression vector was constructed by cloning signal sequence (ss) and the extracellular domain of Robo4 into a pcDNA3.1 vector.

whether Robo4 multimerization can occur independent of any ligands. Further characterization of Robo4 using shRobo4 and smRobo4 is expected to elucidate the role of Robo4 in angiogenesis, which may contribute to the development of novel vessel-targeting therapies.

Materials and methods

cDNA cloning

Full-length cDNA of hRobo4 (GenBank Accession No. NM019055) was purchased from OriGene Technologies Inc. (Rockville, MD), and the full-length cDNA of mRobo4 (GenBank Accession No. NM028783) was kindly provided by Dr. Okada at Osaka University, Japan. The primers used were as follows; hRobo4: forward primer 5′-CACCATGGGCTCTGGAGGAGACAGCCTC-3′, reverse primer 5′-CTCAGGCCGCTTCAAGGTAGCCCT-3′; mRobo4: forward primer 5′-CACCATGGGACAAGGAGAGGAGCCGAG-3′, reverse primer 5′-TGGTCGTCTCAAGGTGGCCCTCA-3′. Using these primers, the extracellular domains (1–469 amino acids of hRobo4 and 1–479 amino acids of mRobo4), containing the signal sequences, were amplified by polymerase chain reaction (PCR). The PCR products were purified by agarose gel extraction using a QIAquick Gel Extraction kit (QIAgen, Valencia, CA). The purified PCR products were directly cloned into pcDNA™3.1D/V5-His-TOPO vectors (Invitrogen Corporation, Carlsbad, CA), which were designed to express the protein with a His-Tag fused to the C-terminal. Cloned cDNA was transformed into competent *Escherichia coli*, *One Shot Top10* (Invitrogen Corporation), and selected on Luria–Bertani agar plates containing 50 μg/mL ampicillin. Coding sequences of these plasmids were confirmed by DNA sequencing analysis using a PRISM 3100-Avant Genetic Analyzer (Applied Biosystems, Bridgewater, CT).

Expression of shRobo4 and smRobo4 in mammalian cells

293F human embryonic kidney cells, adapted to suspension culture, were cultured using FreeStyle™ 293 Expression Medium (Invitrogen Corporation) in an incubator at 37 °C with a humidified atmosphere of 8% CO_2. Flasks containing the cells were rotated at 125 rpm on an orbital shaker (SANYO, Japan). The transfection procedure was performed using the lipofection method with 293 fectin reagent (Invitrogen Corporation). Lipid–DNA complexes were formed by mixing 1 μL or 2 μL 293 fectin and 1 μg DNA per 1 mL cell culture. This complex was added to 100 mL media containing 293F cells at 1×10^6 cells/mL in a 500-mL flask. An aliquot of the cell culture was collected every 24 h and the protein expression levels were assessed by Western blotting. After optimizing the transfection conditions, the culture scale was expanded to a total of 750 mL (three 1-L flasks containing 250 mL media each). The culture was centrifuged at 8000*g* for 10 min to remove the cells, and the resulting supernatant was filtered using 0.45-μm polyvinylidene fluoride membrane (ADVANTEC MFS, Dublin, CA). Clarified supernatants were stored at −80 °C until use in the purification procedure.

Western blotting

Each sample was diluted by the same volume of Laemmli sample buffer (Bio-Rad Laboratories, Inc., San Diego, CA) containing 5% 2-mercaptoethanol (Wako Pure Chemical Industries, Japan) and applied to sodium dodecyl sulfate–polyacrylamide gel electrophoresis (SDS–PAGE). For the anti-His-tag Western blot experiments, 10 μL of cultured supernatants were loaded onto the gels. For the anti-Robo4 Western blot experiments, 100 ng of purified Robo4 was loaded onto the gels. Transferred soluble Robo4 was bound by 6× His monoclonal antibodies (Becton Dickinson and Company, Franklin Lakes, NJ) or anti-Robo4 monoclonal antibody (Santa Cruz Biotechnology, Inc., Santa Cruz, CA), and then detected using anti-mouse IgG and ECL plus reagent (GE Healthcare, UK Ltd.)

Nickel nitrilotriacetic acid (Ni–NTA) purification and gel-filtration chromatography

The Ni–NTA purification step and gel-filtration chromatography were performed using AKTA Crystal (GE Healthcare, UK Ltd.) at 4 °C. Filtered supernatant containing expressed Robo4 was applied to a His-Trap Fast Flow 1-mL column (GE Healthcare, UK Ltd.) equilibrated with binding buffer (20 mM imidazole, 500 mM NaCl, 50 mM Tris–HCl, pH 7.4). After washing with 10 column volumes of binding buffer, bound Robo4 was eluted by 5 column volumes of elution buffer (500 mM imidazole, 500 mM NaCl, and 50 mM Tris–HCl, pH 7.4). Fractions containing protein as determined by the absorbance at 280 nm were directly applied to a HiLoad 16/60 Superdex 200 pg column (GE Healthcare, UK Ltd.) equilibrated with PBS (137 mM NaCl, 2.7 mM KCl, 10 mM Na_2HPO_4, and 1.8 mM KH_2PO_4, pH 7.4). The PBS flow rate was 1 mL/min and 1.5-mL fractions were collected. Fractions containing soluble Robo4 were combined and concentrated using Amicon Ultra filtration cartridges (Millipore Corporation, Billerica, MA). Their purities were assessed by SDS–PAGE and gel-filtration analysis. The protein concentration was determined by Coomassie Plus Protein Assay Reagent (Pierce Biotechnology, Inc., Rockford, IL). Obtained proteins were stored at −80 °C.

Analytical gel-filtration

Analytical gel-filtration was performed using Superdex 200 10/300 GL columns (GE Healthcare, UK Ltd.) at 4 °C with PBS (flow rate = 0.5 mL/min). To determine the molecular size of Robo4, a Gel-filtration Calibration Kit LMW and HMW (GE Healthcare, UK Ltd.) were used as molecular weight markers. Two marker

mixtures were prepared by mixing individual marker proteins. The compositions of the markers were: Marker I, 5 mg/mL ribonuclease A (13.7 kDa), 5 mg/mL ovalbumin (43 kDa), 5 mg/mL aldolase (158 kDa), and 5 mg/mL ferritin (440 kDa); Marker II, 5 mg/mL chymotrypsinogen (25 kDa), 5 mg/mL albumin (67 kDa), and 5 mg/mL catalase (232 kDa). The marker mixtures (10 μL) were each injected onto the column and a standard curve between the molecular weight and the elution time was calculated. The molecular weight of purified soluble Robo4 was calculated based on these standard curves.

Blue Native PAGE

Blue Native PAGE was performed using Native PAGE Novex Bis–Tris Gel System (Invitrogen Corporation). The sample contained 1 μL 5% G-250 sample additive, 1 μL of 10% DDM, and 1 μg Robo4 in 10 μL of 1× Native PAGE Sample Buffer (Invitrogen Corporation). Samples (10 μL per well) were loaded on 4–16% Bis–Tris gels, electrophoresed, and stained. Native Mark Unstained Protein standard (Invitrogen Corporation) was used as the molecular weight marker.

Results

Expression of shRobo4 and smRobo4

The signal sequences and the extracellular domains of hRobo4 and mRobo4 were cloned into pcDNA3.1 vectors to produce a mammalian expression system (Fig. 1). First, we optimized the expression conditions, such as the amount of 293 fectin used as the transfection reagent and the culture duration for a small scale 100-mL culture. The expression of shRobo4 was confirmed using anti-His-Tag Western blotting and bands were detected at 60–75 kDa in the supernatant sample collected on day 6 after transfection (Fig. 2A). The shRobo4 expression level in the 2-μL/mL culture condition was slightly higher. Therefore, the expression of smRobo4 was performed using the 2-μL/mL culture condition and confirmed to be similar to that of shRobo4 (Fig. 2B). The soluble Robo4 bands were broad and migrated at a higher molecular weight than expected, which may have been due to glycosylation. Under the optimized conditions, the culture scale was expanded up to 750 mL (shRobo4) or 500 mL (smRobo4).

Purification

Purification of shRobo4 and smRobo4 was performed by two-step chromatography (Ni–NTA and gel-filtration). The peak Robo4 fraction was observed using imidazole for elution from the Ni–NTA column (Fig. 3A and C). Fractions with an absorbance greater than 20 mAU were collected as the peak fractions, pooled, and automatically injected onto the gel-filtration column. A single peak was observed and equally sized fractions were collected (Fig. 3B and D). The fractions corresponding to the peak were concentrated and the purity was checked using Coomassie Brilliant blue staining following SDS–PAGE (Fig. 4A). Loading of 1 μg purified protein produced a single broad band without residual contamination. The band was confirmed to be soluble Robo4 using anti-Robo4 Western blotting with 100 ng protein (Fig. 4B). In the figure, the band looks partially white due to saturation of the reaction. These results indicate that shRobo4 and smRobo4 were successfully purified without any aggregation. The final yields of shRobo4 and smRobo4 were 1 mg

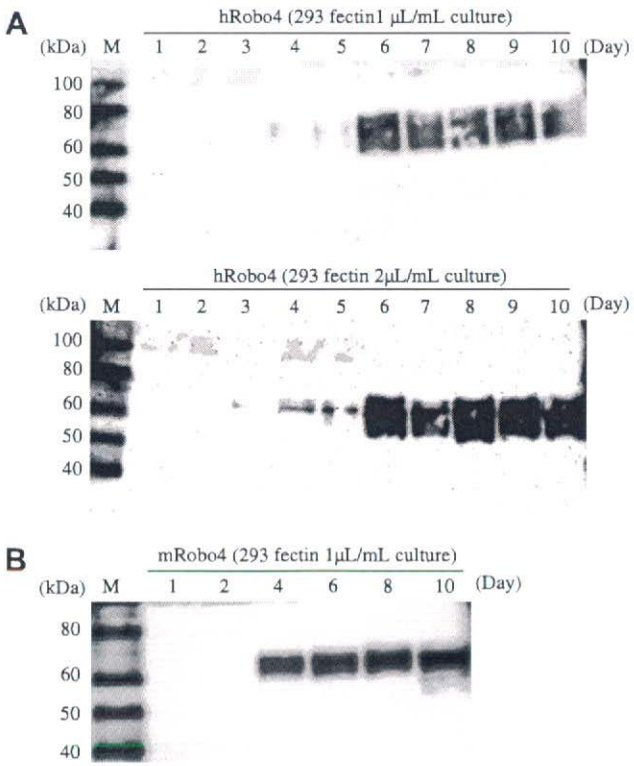

Fig. 2. The time course of the expression of shRobo4 and smRobo4. The transfection experiment in a small scale culture was performed to optimize the concentration of 293 fectin and to determine the culture duration needed to reach an adequate expression level. (A) Expression pattern of shRobo4. The transfection was performed using 1 μL 293 fectin/1 mL culture or 2 μL 293 fectin/1 mL culture. The culture supernatant was collected every 24 h post-transfection and shRobo4 expression was checked by anti-His-tag Western blotting. (B) Expression pattern of smRobo4. Transfection was performed using 2 μL 293 fectin/1 mL culture. The culture supernatant was collected every 48 h post-transfection starting on day 1 and the expression level was checked by anti-His-tag Western blotting.

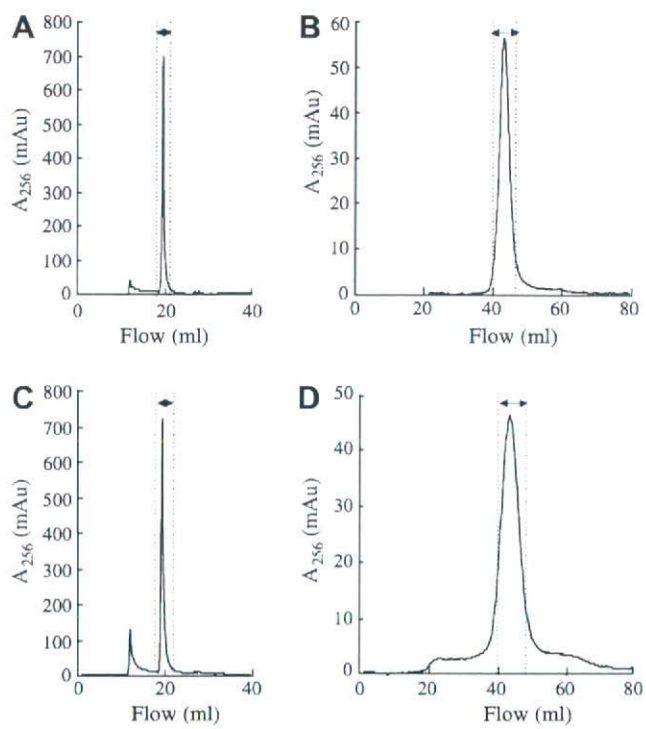

Fig. 3. Purification of shRobo4 and smRobo4. shRobo4 (A and B) and smRobo4 (C and D) were purified by two-step chromatography using Akta Crystal. Gel-filtration was performed followed by Ni–NTA purification. The protein concentration in the flow path was monitored at 254 nm through Ni–NTA (A and C) and gel-filtration (B and D). The eluted fractions corresponding to the main peak (between dashed lines) were collected.

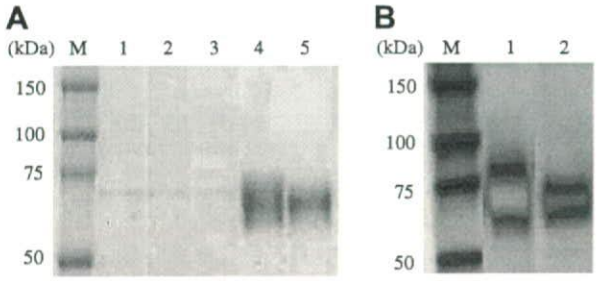

Fig. 4. Purity check and quality assessment of the purified shRobo4 and smRobo4. (A) Purity verification of shRobo4 and smRobo4 with Coomassie blue staining. Lane M: Precision Kaleidoscope Protein Standard (kDa), Lane 1: supernatant of non-treated 293 F, Lane 2: supernatant of shRobo4-expressing cells, Lane 3: supernatant of smRobo4-expressing cells, Lane 4: purified shRobo4, Lane 5: purified smRobo4. Supernatants (Lanes 1–3) were loaded at 10 μL/lane. The protein concentration of purified Robo4 (Lanes 4–5) was determined and the purified samples were loaded at 1 μg protein/lane. (B) Anti-Robo4 Western blotting of purified shRobo4 and smRobo4. Lane M: Precision Kaleidoscope Protein Standard (kDa), Lane 1: purified shRobo4, Lane 2: purified smRobo4. Each purified sample (Lanes 1 and 2) was loaded at 100 ng protein/lane.

from a 750-mL culture (shRobo4) and 520 μg from a 500-mL culture (smRobo4; Table 1).

Analysis of shRobo4 and smRobo4 multimerization

To examine the ligand-independent multimerization of Robo4, we calculated the native molecular weight using analytical gel-filtration and Blue Native PAGE. Analytical gel-filtration was performed using seven different native proteins as the molecular weight standard (Fig. 5A). The retention times of shRobo4 and smRobo4 were 23.5 min and 24.5 min, respectively (Fig. 5B and C). Calculated molecular weights of shRobo4 and smRobo4 were 216 kDa and 180 kDa, respectively. Similar results were obtained with Blue Native PAGE (Fig. 5D). Both shRobo4 and smRobo4 were detected as single broad bands at over 200 kDa. The molecular weights of the Robo4 monomers were 60–75 kDa, based on the SDS–PAGE results (Fig. 4A and B), suggesting that Robo4 assembles into a multimer independent of its ligand.

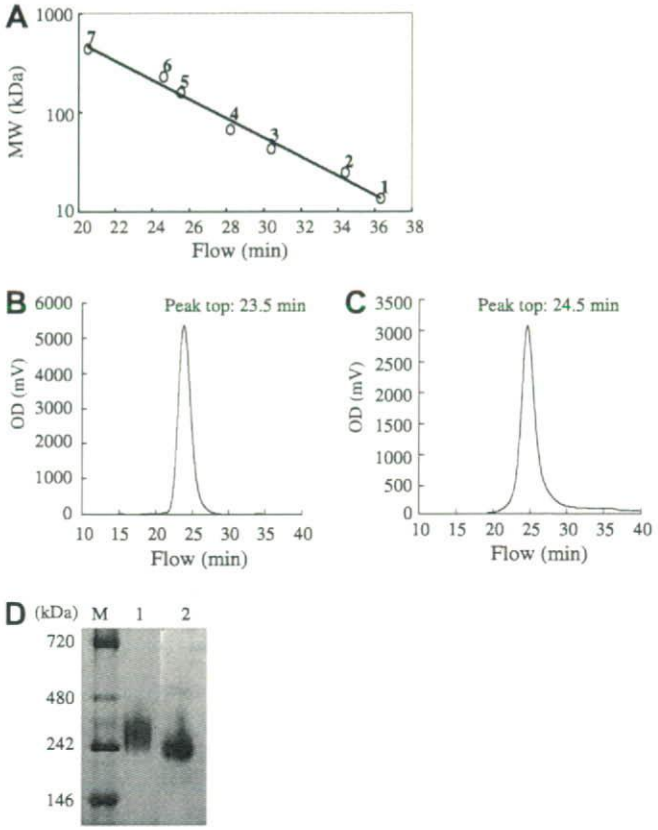

Fig. 5. Calculation of native molecular weight of shRobo4 and smRobo4. (A–C) Analytical gel-filtration of Robo4 s. (A) The standard curve was prepared using an L&H MW GF calibration kit. This kit consists of Marker 1 (1, ribonuclease, 13.7 kDa; 3, ovalbumin, 43 kDa; 5, aldolase, 158 kDa; 7, ferritin, 440 kDa) and Marker 2 (2, chymotrypsinogen, 25 kDa; 4, albumin, 67 kDa; 6, catalase, 232 kDa). (B) The peak of shRobo4. (C) The peak of smRobo4. Native molecular weights were calculated from the standard curve. (D) Blue Native PAGE using purified shRobo4 and smRobo4. The molecular size of native Robo4 was estimated using a Native Mark™ unstained protein standard (Lane M). Lane 1: shRobo4, Lane 2: smRobo4. Each protein was loaded at 1 μg/lane.

Discussion

Here, we established an expression and purification method for soluble human and mouse Robo4, which is an important molecule for embryonic and tumor angiogenesis. Using this method, we successfully obtained highly purified shRobo4 and smRobo4 in yields over 1 mg/L. For higher yields, another effective transfection reagent and cell type may be beneficial, as previously reported [17–19].

In SDS–PAGE analysis, purified shRobo4 and smRobo4 were detected as a broad band at a position 20 kDa higher than the theoretical molecular weight determined from its amino acid structure. This might be a result of protein glycosylation as proteins expressed in mammalian cells are often highly glycosylated [20,21]. Analysis of the protein sequence (Swiss-Prot entry Q8WZ75) suggests that the asparagines at amino acids 246, 360, 389, and 396 of hRobo4 are potential N-linked glycosylation sites, but this was not confirmed in the present study. Interestingly, our results indicated that the band for shRobo4 was broader than that for smRobo4, which may be due to a difference in the type of glycosylation between shRobo4 and smRobo4, despite their high sequence homology (>80%) [2].

Table 1
The yield of purified shRobo4 and smRobo4

	Culture volume	Yield
shRobo4	250 mL × 3	1.33 mg/1L culture
smRobo4	250 mL × 2	1.04 mg/1L culture

Based on analytical gel-filtration and BN-PAGE, the native molecular weight of soluble Robo4 was calculated to be over 200 kDa, which suggests that soluble Robo4 assembled into multimers in the absence of its ligands. Protein multimerization is important for protein function, including signal initiation [22,23]. In particular, multimerization may enhance Robo4 signaling and function [5,16]. Although the production of human Robo4-Fc chimeric protein, artificially dimerized by the Fc portion, was reported [7], there has been no previous report of Robo4 self-assembly. The novel finding of the present study that Robo4 can self-assemble in the absence of its ligands may be useful for identifying the Robo4 ligand. It is not known whether soluble Robo4 binds to the Robo1–3 ligands (especially slit members), but the Robo1–3 ligands do not bind to the Robo4-Fc chimeric protein.

Thus, the purified shRobo4 and smRobo4 will facilitate further Robo4 characterization studies, such as the search for the Robo4 ligand and the analysis of Robo4 function. Clarification of Robo4 function and its role in angiogenesis may contribute to advance basic research on vasculature. In addition, X-ray structural analysis of soluble Robo4 will advance the drug discovery process for anti-neoangiogenesis therapy. The expression and purification method for soluble Robo4 proteins developed in the present study

is expected to be an important component of many basic and therapeutic studies of Robo4.

Acknowledgments

This study was supported by the Japan Science and Technology Agency (JST), Research Fund Project on Health Sciences focusing on Drug Innovation (No. KAA3701) from the Japan Health Sciences Foundation, and in part by Grant-in-Aid for Young Scientists (B) (No. 20790134) from the Ministry of Education, Culture, Sports, Science and Technology of Japan (MEXT) and Japan Society for the Promotion of Science (JSPS).

References

[1] L. Huminiecki, R. Bicknell, In silico cloning of novel endothelial-specific genes, Genome Res. 10 (2000) 1796–1806.
[2] L. Huminiecki, M. Gorn, S. Suchting, R. Poulsom, R. Bicknell, Magic roundabout is a new member of the roundabout receptor family that is endothelial specific and expressed at sites of active angiogenesis, Genomics 79 (2002) 547–552.
[3] W. Andrews, M. Barber, L.R. Hernadez-Miranda, J. Xian, S. Rakic, V. Sundaresan, T.H. Rabbitts, R. Pannell, P. Rabbitts, H. Thompson, L. Erskine, F. Murakami, J.G. Parnavelas, The role of Slit-Robo signaling in the generation migration, and morphological differentiation of cortical interneurons, Dev. Biol. 313 (2008) 648–658.
[4] A.K. Challa, C.E. Beattie, M.A. Seeger, Identification and characterization of roundabout orthologs in zebrafish, Mech. Dev. 101 (2001) 249–253.
[5] V.M. Bedell, S.Y. Yeo, K.W. Park, J. Chung, P. Seth, V. Shivalingappa, J. Zhao, T. Obara, V.P. Sukhatme, I.A. Drummond, D.Y. Li, R. Ramchandran, Roundabout4 is essential for angiogenesis in vivo, Proc. Natl. Acad. Sci. USA 102 (2005) 6373–6378.
[6] J. Grone, O. Doebler, C. Loddenkemper, B. Hotz, H.J. Buhr, S. Bhargava, Robo1/Robo4: differential expression of angiogenic markers in colorectal cancer, Oncol. Rep. 15 (2006) 1437–1443.
[7] S. Suchting, P. Heal, K. Tahtis, L.M. Stewart, R. Bicknell, Soluble Robo4 receptor inhibits in vivo angiogenesis and endothelial cell migration, FASEB J. 19 (2005) 121–123.
[8] P. Seth, Y. Lin, J. Hanai, V. Shivalingappa, M.P. Duyao, V.P. Sukhatme, Magic roundabout a tumor endothelial marker: expression and signaling, Biochem. Biophys. Res. Commun. 332 (2005) 533–541.
[9] K.W. Park, C.M. Morrison, L.K. Sorensen, C.A. Jones, Y. Rao, C.B. Chien, J.Y. Wu, L.D. Urness, D.Y. Li, Robo4 is a vascular-specific receptor that inhibits endothelial migration, Dev. Biol. 261 (2003) 251–267.
[10] B. Wang, Y. Xiao, B.B. Ding, N. Zhang, X. Yuan, L. Gui, K.X. Qian, S. Duan, Z. Chen, Y. Rao, J.G. Geng, Induction of tumor angiogenesis by Slit-Robo signaling and inhibition of cancer growth by blocking Robo activity, Cancer Cell 4 (2003) 19–29.
[11] M. Gorn, M. Anige, I. Burkholder, B. Muller, A. Scheffler, L. Edler, I. Boeters, J. Panse, G. Schuch, D.K. Hossfeld, E. Laack, Serum levels of Magic Roundabout protein in patients with advanced non-small cell lung cancer (NSCLC), Lung Cancer 49 (2005) 71–76.
[12] W. Yuan, L. Zhou, J.H. Chen, J.Y. Wu, Y. Rao, D.M. Ornitz, The mouse SLIT family: secreted ligands for ROBO expressed in patterns that suggest a role in morphogenesis and axon guidance, Dev. Biol. 212 (1999) 290–306.
[13] M. Fujiwara, M. Ghazizadeh, O. Kawanami, Potential role of the Slit/Robo signal pathway in angiogenesis, Vasc. Med. 11 (2006) 115–121.
[14] J.A. Legg, J.M. Herbert, P. Clissold, R. Bicknell, Slits and roundabouts in cancer, tumour angiogenesis and endothelial cell migration, Angiogenesis (2008).
[15] C. Morlot, N.M. Thielens, R.B. Ravelli, W. Hemrika, R.A. Romijn, P. Gros, S. Cusack, A.A. McCarthy, Structural insights into the Slit–Robo complex, Proc. Natl. Acad. Sci. USA 104 (2007) 14923–14928.
[16] S. Kaur, M.D. Castellone, V.M. Bedell, M. Konar, J.S. Gutkind, R. Ramchandran, Robo4 signaling in endothelial cells implies attraction guidance mechanisms, J. Biol. Chem. 281 (2006) 11347–11356.
[17] C. Liu, B. Dalby, W. Chen, J.M. Kilzer, H.C. Chiou, Transient transfection factors for high-level recombinant protein production in suspension cultured mammalian cells, Mol. Biotechnol. (2008).
[18] P. Hawley-Nelson, V. Ciccarone, M.L. Moore, Transfection of cultured eukaryotic cells using cationic lipid reagents, in: F.M. Ausubel, R. Brent, R.E. Kingston, D.D. Moore, J.G. Seidman, J.A. Smith, K. Struhl (Eds.), Current Protocols in Molecular Biology, John Wiley & Sons, Inc., New York, 2008 (Chapter 9, Unit 9.4).
[19] R.G. Werner, W. Noe, K. Kopp, M. Schluter, Appropriate mammalian expression systems for biopharmaceuticals, Arzneimittelforschung 48 (1998) 870–880.
[20] R.G. Werner, K. Kopp, M. Schlueter, Glycosylation of therapeutic proteins in different production systems, Acta Paediatr. Suppl. 96 (2007) 17–22.
[21] J.P. Gaudry, C. Arod, C. Sauvage, S. Busso, P. Dupraz, R. Pankiewicz, B. Antonsson, Purification of the extracellular domain of the membrane protein GlialCAM expressed in HEK and CHO cells and comparison of the glycosylation, Protein Expr. Purif. 58 (2008) 94–102.
[22] C. Ruch, G. Skiniotis, M.O. Steinmetz, T. Walz, K. Ballmer-Hofer, Structure of a VEGF–VEGF receptor complex determined by electron microscopy, Nat. Struct. Mol. Biol. 14 (2007) 249–250.
[23] F. Mac Gabhann, A.S. Popel, Dimerization of VEGF receptors and implications for signal transduction: a computational study, Biophys. Chem. 128 (2007) 125–139.

J Hum Genet (2008) 53:1012–1015
DOI 10.1007/s10038-008-0336-5

SHORT COMMUNICATION

LRRK2 P755L variant in sporadic Parkinson's disease

Hiroyuki Tomiyama · Ikuko Mizuta · Yuanzhe Li · Manabu Funayama · Hiroyo Yoshino · Lin Li · Miho Murata · Mitsutoshi Yamamoto · Shin-ichiro Kubo · Yoshikuni Mizuno · Tatsushi Toda · Nobutaka Hattori

Received: 20 June 2008 / Accepted: 31 August 2008 / Published online: 16 October 2008

Abstract Parkinson's disease (PD) is a neurodegenerative disorder of unknown etiology with probable involvement of genetic-environmental factors. The majority of PD cases (approximately 90–95%) are sporadic, while familial cases account for approximately 5–10% of PD. In a recent report, a heterozygous *LRRK2* P755L mutation within *LRRK2* exon 19 was found in 2% of Chinese sporadic PD patients and in 0% of normal controls or Caucasians, suggesting that the mutation is disease-associated with ethnic specificity. To further evaluate the role of *LRRK2* P755L variant in sporadic PD, we performed direct sequencing of *LRRK2* exon 19 in 501 Japanese sporadic PD patients (male 249, female 252, aged 28–92 years, mean 65.0 years) and 583 controls of the Japanese general population as an extended association study. In this group, we found six patients (6/501 = 1.2%) and eight controls of the general population (8/583 = 1.6%) with a heterozygous P755L variant ($P = 0.80$, $\chi^2 = 0.064$). No other variants were found in exon 19. Together with previous reports, our extended case-controlled study of large sample size suggests that *LRRK2* P755L is a non-disease-associated polymorphism in PD patients.

Keywords Parkinson's disease · Genetics · *PARK8* · *Leucine-rich repeat kinase 2 (LRRK2)* · Polymorphism · Association study · Japanese · Ethnic background

H. Tomiyama · Y. Li · L. Li · S.-i. Kubo · N. Hattori (✉)
Department of Neurology,
Juntendo University School of Medicine,
2-1-1 Hongo, Bunkyo-ku, Tokyo 113-8421, Japan
e-mail: nhattori@med.juntendo.ac.jp

I. Mizuta · T. Toda
Division of Clinical Genetics,
Osaka University Graduate School of Medicine,
Suita, Japan

I. Mizuta · M. Murata · M. Yamamoto · T. Toda · N. Hattori
Core Research for Evolutional Science and Technology (CREST), Japan Science and Technology Agency,
Saitama, Japan

M. Funayama · H. Yoshino · Y. Mizuno
Research Institute for Diseases of Old Age,
Juntendo University School of Medicine, Tokyo, Japan

M. Murata
Department of Neurology, Musashi Hospital,
National Center of Neurology and Psychiatry, Tokyo, Japan

M. Yamamoto
Department of Neurology,
Kagawa Prefectural Central Hospital, Takamatsu, Japan

Introduction

Parkinson's disease (PD, OMIM #168600) is the second most common neurodegenerative disorder next to Alzheimer's disease. The clinical features are characterized by levodopa-responsive parkinsonism, such as rigidity, resting tremor, bradykinesia, and postural instability. Although the cause of PD remains unclear, genetic-environmental interaction is suggested for the development of the disease. One of the autosomal-dominant forms of PD, *PARK8*, was originally mapped from a Japanese Sagamihara family (Funayama et al. 2002) and *LRRK2* (*PARK8*; *leucine-rich repeat kinase 2*, OMIM *609007) was identified as the causative gene for *PARK8*-linked PD (Paisán-Ruíz et al. 2004; Zimprich et al. 2004). Among *LRRK2* mutations, the most common *LRRK2* G2019S mutation in North Africans and Ashkenazi Jews has shown ethnic differences among Caucasian, Japanese, and Chinese (Nichols et al. 2005; Gilks et al. 2005; Lesage et al. 2006; Tomiyama et al.